STUDIES IN THE MASS 160 DECAY CHAIN. GAMMA-RAY AND CONVERSION ELECTRON SPECTROSCOPY FOR THE ^{160}LU $\rightarrow$ ^{160}YB, ^{160}YB $\rightarrow$ ^{160}TM, ^{160}TM $\rightarrow$ ^{160}ER DECAY SCHEMES.

A Thesis
Presented to
The Academic Faculty

by

Nathaniel J. Brown

In Partial Fulfillment
of the Requirements for the Degree
Doctor of Philosophy in
Physics

School of Physics
Georgia Institute of Technology
May 2009

STUDIES IN THE MASS 160 DECAY CHAIN. GAMMA-RAY AND CONVERSION ELECTRON SPECTROSCOPY FOR THE ^{160}LU $\rightarrow$ ^{160}YB, ^{160}YB $\rightarrow$ ^{160}TM, ^{160}TM $\rightarrow$ ^{160}ER DECAY SCHEMES.

Approved by:

Dr. John L. Wood, Advisor
School of Physics
Georgia Institute of Technology

Dr. W. David Kulp
School of Physics
Georgia Institute of Technology

Dr. A. Turgay Uzer
School of Physics
Georgia Institute of Technology

Dr. Robert A. Braga
Department of Chemistry
Georgia Institute of Technology

Dr. Brian Kennedy
School of Physics
Georgia Institute of Technology

Date Approved: 2008

To my family and friends

for their support and guidance.

ACKNOWLEDGEMENTS

I am sincerely thankful for the assistance, support and help of my family, friends, collaborators, and mentors who have assisted me both in this endeavor and on the path which led me to this point.

I would like to thank John Wood most of all. His tireless efforts created a unique learning environment. His ability to arrange ideas into cohesive thoughts enabled work to be done at the proper pace. The combination of these traits allowed an interested student the opportunity to fly with the eagles, and every student should be so lucky.

I would like to thank David Kulp for his patience and advise. He contributed many images to this thesis and many thoughts to steer me in the right direction. I value his guidance and opinions and have throughly enjoyed working with him.

I would like to thank my parents Mary Patricia and Richard R. Brown Jr. for their unwaivering support and patience. They prepared a loving household that was a joy to grow up in. They nurtured my imagination and encouraged me in every pursuit i have undertaken. The ability to walk this long road is born of strength learned watching my parents succeed in their lives. I would like to thank my brother Jeremiah, my sister in law Candice and my sister Elizabeth, for their unique ability to see the best in me, and offer advise allowing me to walk the path, i could not have done it without you.

I would like to thank Mitch Allmond for his advice and friendship. The ability to have detailed conversation among your peers hones the edges of thoughts and presentations in a very beneficial manner.

The combination of these efforts and many others i haven't mentioned (Columbus, Shadow, Lucky and Bell my four furry friends among them), showed me a path to success. It is my

honor and privilege to have finished this work with help from such wonderful friends and colleagues.

Nathaniel Joseph Brown

TABLE OF CONTENTS

LIST OF TABLES

LIST OF FIGURES

SUMMARY

Excited states in the transitional nucleus $^{160}_{90}$Yb have been studied using γ-ray and conversion electron spectroscopy following the $\beta+$/EC decay of $^{160}_{71}$Lu. Excited states in the nuclei $^{160}_{89}$Tm and $^{160}_{88}$Er have been studied following the $\beta+$/EC decay of $^{160}_{70}$Yb and $^{160}_{89}$Tm, respectively. The data for the present study were obtained at TRIUMF in Vancouver, Canada at the ISAC-1 facility through radioactive sources moved into the combination of the 8π γ-ray spectrometer array and the Pentagonal Array for Conversion Electron Spectroscopy (PACES). Analysis of γ-ray gated γ-ray, γ-ray gated conversion electron and conversion electron gated γ-ray spectra resulted in the discovery of a new first excited state and the establishment of a level scheme for ^{160}Tm which differs from the one adopted; as well as a test of the rotational characteristics of ^{160}Er with intensity comparisons to both the spin-5 β-decaying isomer study of by Singh et al. and the spin-parity 1^- β decay study of by Strusny et al. and Bykov et al.

One of the motivations for this study was to examine excited states above 1 MeV in ^{160}Yb. Previous studies of the excited states of ^{152}Sm and ^{154}Gd revealed structural similarities between the $N = 90$ nuclei near β stability. These nuclei are near a transitional region between spherical and deformed nuclear shapes. The use of the 8π + PACES combination marks the first time that a large Compton-suppressed detector array plus conversion electron detection has been used to study ^{160}Yb.

This study was further motivated by the challenge of demonstrating the feasibility of complex decay scheme spectroscopy far from stability: to this end the ^{160}Yb $\rightarrow$ ^{160}Tm decay scheme has been investigated with the limitation that the decay branches are only elucidated down to the 1 percent level.

Finally, new information on band mixing in ^{160}Er, based on γ-ray intensities observed in the ^{160m,g}Tm $\rightarrow$ ^{160}Er decay scheme, is presented.

CHAPTER I

INTRODUCTION

The initial motivation of this study was the identification of the structural properties that contribute to understanding the nuclear shape of the $N = 90$ nucleus ^{160}Yb. The adopted level schemes of the $N = 90$ nuclei ($^{152}_{62}\mathrm{Sm}_{90}$, $^{154}_{64}\mathrm{Gd}_{90}$, and $^{156}_{66}\mathrm{Dy}_{90}$) near β stability, are nearly identical. Study of the β decay of $^{160}_{71}\mathrm{Lu}_{89}$ to $^{160}_{70}\mathrm{Yb}_{90}$ can provide excited state information which extends this knowledge of a transitional region between spherical and deformed nuclear shapes. Studies of excited states in ^{160}Tm and ^{160}Er have also been carried out with high-statistics spectroscopy, additionally available in the mass-separated beam of spallation products used to study the β decay of ^{160}Lu to ^{160}Yb.

Previous studies of ^{160}Yb were carried out using mainly one or two Ge(Li) γ-ray detectors. The two principal studies used as references [1] for the $T_{1/2} = 36, 40$ sec decay of ^{160}Lu were carried out 34 years ago by et al. [3] with two Ge(Li) detectors and 35 years ago by Gelletly et al. [5] with a Ge(Li) detector and a LEPS (Low-energy photon spectrometer) detector.

The principal study used as a reference [1] for the $T_{1/2} = 4.8$ min β-decaying ground state of ^{160}Yb to ^{160}Tm was done 40 years ago by Schilling et al. [6] using Ge(Li) detectors, toroidal and magnetic-lens β-spectrometers and scintillation counters.

The principal studies used as references [1] for the two β-decaying isomers proposed in the decay of ^{160}Tm to ^{160}Er were carried out by Strusny et al. [7], Bykov et al. [8], and Singh et al. [9]. The $T_{1/2} = 9.4$ min decay was studied by Strusny using a combination of Ge(Li) detectors and conversion electron detection using a magnetic spectrograph (for multipolarity information). The decay study of Bykov was done using "total-absorption" γ-ray spectroscopy, with a system of three NaI(Tl) detectors. Singh used three high-resolution Ge detectors and a mini-orange spectrometer with a cooled Si(Li) detector for collecting

internal-conversion electron spectra to study the $T_{1/2} = 74.5$ sec isomeric decay from a spin-5 state. Recently, excited states in ^{160}Er have been studied by Dusling [10] using the ^{159}Tb (^{6}Li,5n) reaction (in beam). This study observes high-spin states, and the only overlap with the present work is for the ground-state band to spin $J = 6$.

The theories that best describe the nuclei in the $N = 90$ region are discussed in chapter 2.

CHAPTER II

BASIC NUCLEAR STRUCTURE THEORY

2.1 Shell Model

The shell model is the most fundamental nuclear structure model. It describes a nucleon, proton or neutron, moving independently in a potential well generated by all the other nucleons. This model uses as a first-order approximation for the nuclear potential, V, a three dimensional isotropic harmonic oscillator potential,

$$V(x,y,z) = \frac{mw^2}{2}(x^2+y^2+z^2). \tag{1}$$

This potential, combined with the kinetic energy, creates a separable Hamiltonian of the form:

$$H(x,y,z) = \frac{1}{2m}(p_x^2+p_y^2+p_z^2) + \frac{mw^2}{2}(x^2+y^2+z^2). \tag{2}$$

The separable solutions of this system take the form

$$E_N = (N+\frac{3}{2})\hbar w; \tag{3}$$

with available states

$$|n_x n_y n_z\rangle, \tag{4}$$

where $N = n_x+n_y+n_z$ is the total number of quanta, and n_x, n_y and n_z are positive integers or zero. Since protons and neutrons are also fermions, the energy states the nucleons occupy are filled up to the Fermi energy, as nucleons are added to the nucleus. The nucleons fill these energy states with definite total angular momentum. There are separate energy levels for protons and neutrons. The ground state $|n_x n_y n_z\rangle$ of a nucleus has each of its protons and neutrons in the lowest energy level allowed by the Pauli exclusion principle. This fermionic nature leads to energy gaps in the system, which result in shell closures for nucleon number, also called magic numbers, of $(2, 8, 20, 40, 70, 112, 168, ...)$. These predictions were seen not to hold true experimentally, pointing to missing physics.

An additional term, $C(\vec{l}\cdot\vec{s})$, where C is determined empirically, suggested independently by Mayer [16], and by Haxel, Suess, and Jensen[17], removes the degeneracy in the orbital angular momentum. Thus, values of the harmonic oscillator shells are modified giving the experimentally observed values: $2, 8, 20, 28, 50, 82, 126, ...$ The modified energy levels therefore appear as

$$E_N = (N + \frac{3}{2})\hbar w + \frac{1}{2}C((j(j+1) - l(l+1) - s(s+1))\hbar^2. \tag{5}$$

This provides the basic microscopic view of the nucleus. It is most effective when applied to nuclei near closed shell and subshell values of the nucleon number. However, it fails to account for the electric quadrupole moments measured in mid-shell regions. Static measured values are much larger than shell model estimates. The reason is that the shell model neglects deformations of the nucleus.

2.2 Bohr Collective Model

The Bohr collective model [15] describes the nucleus as a deformable liquid drop. The nuclear surface can be described by expressing the nuclear radius in the form

$$R(\theta,\phi,t) = R_o\left(1+\sum_{\lambda=0}^{\infty}\sum_{\mu=-\lambda}^{\lambda}\alpha^*_{\lambda,\mu}(t)Y_{\lambda,\mu}(\theta,\phi)\right), \tag{6}$$

with time-dependent shape parameters, $\alpha_{\lambda,\mu}$, and the spherical harmonics, $Y_{\lambda,\mu}(\theta,\phi)$. The dominating spherical harmonics are those with $\lambda = 2$.

The first of two degrees of freedom allowed in the collective model are vibrations, where the nuclear shape is free to oscillate around a spherical equilibrium shape. The Hamiltonian is

$$H^{\text{Quad}}_{\text{Vib}} = \frac{\Pi^2}{2B} + \frac{1}{2}C\alpha^2_{2,\mu}, \tag{7}$$

with $\mu = 2,1,0,-1,-2$, Π is the momentum canonical to α, B is the inertia parameter and C is the rigidity with respect to the oscillations. This describes a five-dimensional isotropic harmonic oscillator, therefore the energy spectrum is

$$E_N = (N+\frac{5}{2})\hbar w, \tag{8}$$

and the eigenstates are

$$|N\lambda\mu\rangle, \lambda = 2, \mu = 2,1,0,-1,-2. \tag{9}$$

A short discussion of the quanta carried by $\lambda = 2$ is given here. The states produced by these vibrational excitations, are characterized by N, the number of quadrupole oscillator quanta, and $w = \sqrt{\frac{C}{B}}$, the frequency of oscillations. The "m scheme" arranges the possible combinations of quanta allowed. With each oscillator quantum having angular momentum $\lambda = 2$, the $N = 2$ phonons combine to produce total angular momenta $J = 0,2,4$.

The second degree of freedom is rotation. This is represented by a frozen object with a rigid shape, only without a rigid moment of inertia. The resulting Hamiltonian is

$$H_{Rot} = \sum_i \frac{I_i^2}{2g_i} \tag{10}$$

with $i = (1,2,3)$ and axial symmetry $g_1 = g_2 \neq g_3$, where I_i is the total angular momentum and g_i the moments of inertia.

If the deformed frozen shape is relaxed, quadrupole shapes possess two principal modes of vibration, $(Y_{2,2}+Y_{2,-2})$-modes (called γ vibrations) and $Y_{2,0}$-modes (called β vibrations). The occurrence of these modes at low energy in nuclei is in doubt [18]; however, it is convenient to refer to the lowest $K^\pi = 0^+$ and 2^+ bands as β bands and γ bands, respectively.

The collective model has been very successful in describing a variety of nuclear properties, especially energy levels in nuclei with an even number of protons and neutrons. Nuclei with an even nucleon number have few low-lying energy states due to a pairing energy gap. These nuclei can be treated as having no valence particles so that the shell model is not needed. These energy levels display the characteristics of either a rotating or vibrating system.

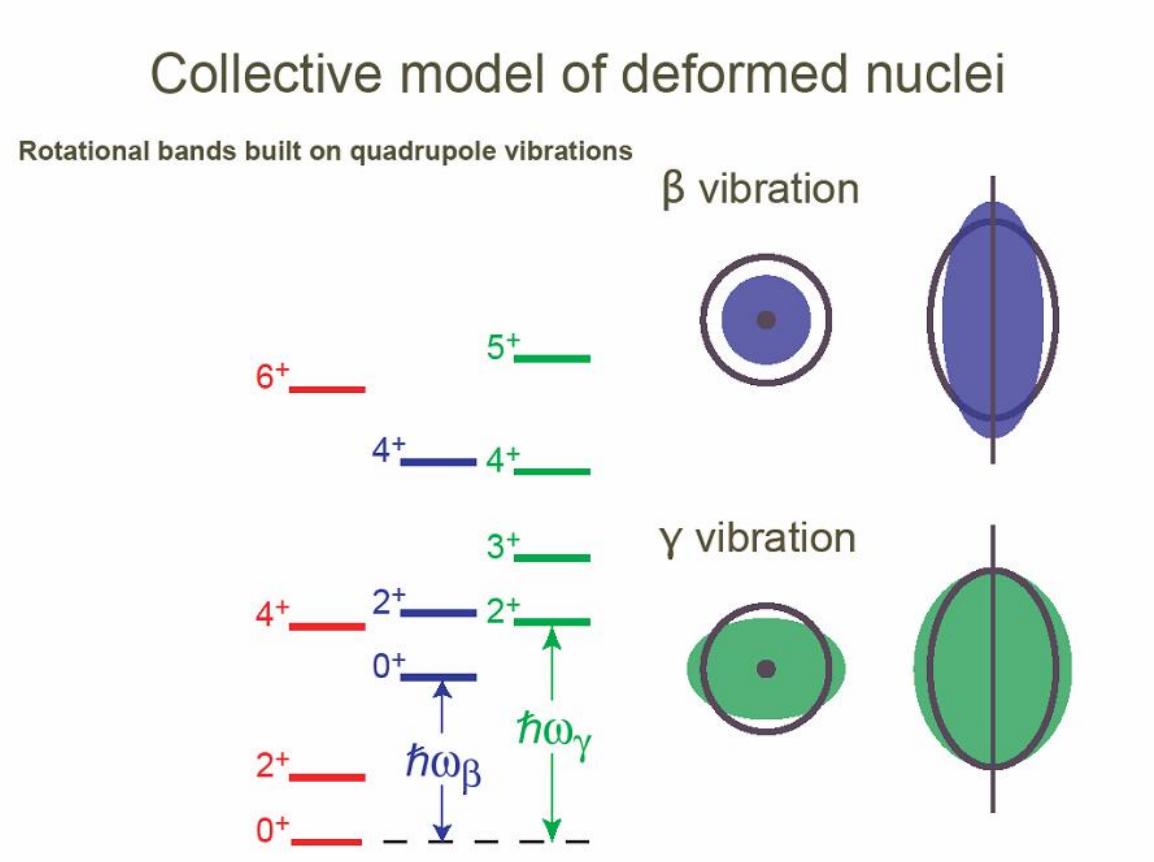

Figure 1: Pictorial representation of rotational band structure built upon two different vibrational excitations.

The β vibration preserves axial symmetry while elongating the principal axis in a stretching mode. The γ vibration does not preserve axial symmetry, and is represented as deforming the principal axis in a "'squishing"' mode (the nuclear shape is flattened in both axial dimensions).

Figure 2 illustrates the effect deformation has on the ground state band energy levels, it displays the $N = 90$ nuclei plotted using the $\frac{E(4^+)}{E(2^+)}$ ratio on the y-axis and mass number on the x-axis.

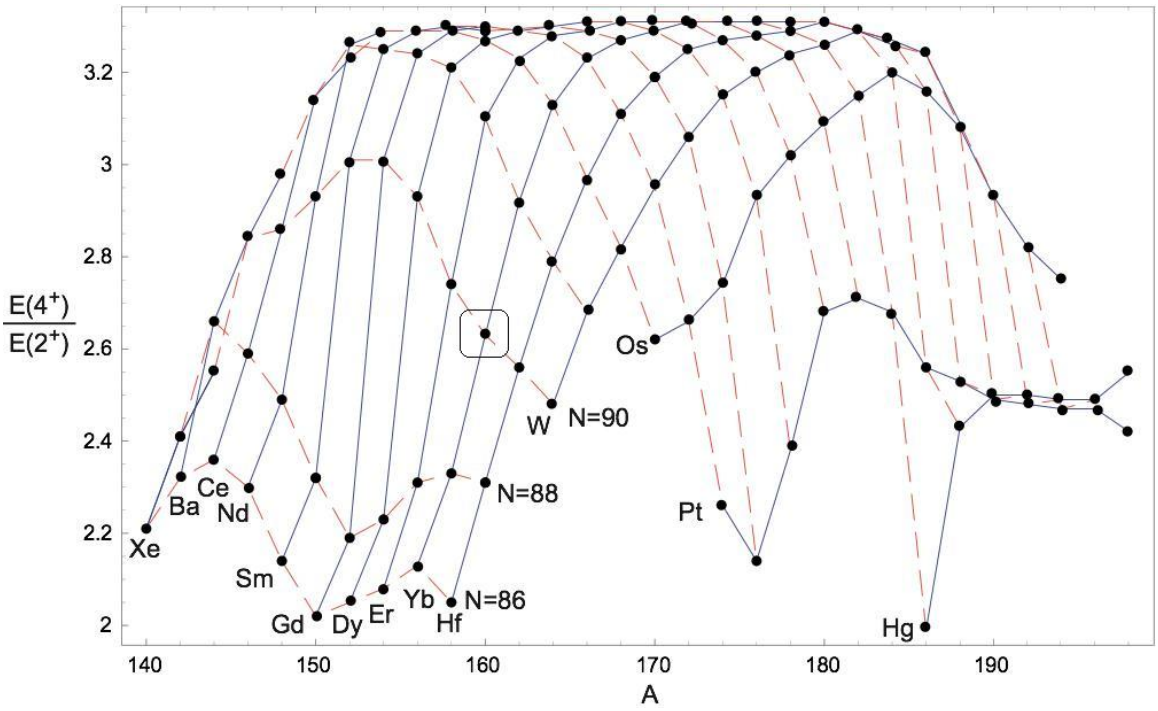

Figure 2: A simple view of collectivity using the ratio $\frac{E(4^+)}{E(2^+)}$ graphed on the y-axis and, the mass number on the x-axis. The nucleus $^{160}_{70}$Yb is marked with a square.

The top of Figure 2 represents the rotational limit for the $\frac{E(4^+)}{E(2^+)} \approx 3.33$ ratio. The bottom is the vibrational limit $\frac{E(4^+)}{E(2^+)} \approx 2$. ^{160}Yb is seen near the middle in Figure 2, accented with a square. One can see the onset of deformation this region of nuclei undergo when $N = 90$ is approached. For the $N = 90$ nuclei near stability this ratio is near the rotational limit of 3.3, as opposed to the vibrational limit of 2.0.

Figure 2 reveals nuclei with a substantial shape change between $N = 88$ and $N = 90$. Evidence of this was analyzed previously, Kulp et al. [18] in the $^{152}_{62}$Sm and $^{154}_{64}$Gd region. $^{160}_{70}$Yb displays a similar, albeit less drastic, shift between vibrational (spherical) to rotational (deformed) nuclear shape between $N = 88$ and $N = 90$.

The nucleus ^{156}Yb in the ($N = 86$) nuclide is best described as a spherical nucleus. A deformation is observed as the neutron number increases through $N = 90$. Large deformation is seen by $N = 94$ or ^{164}Yb and continues into more neutron rich nuclei.

2.2.1 The Rotor Model

The rotor model describes deformed even-even nuclei and is a submodel of the Bohr model. This model can provide algebraic solutions for transition strengths and it yields selection rules. The quantum numbers of the rotor model are shown in Figure 3. This assumes a near symmetric deformed shape. A further assumption of adiabatic rotations is made.

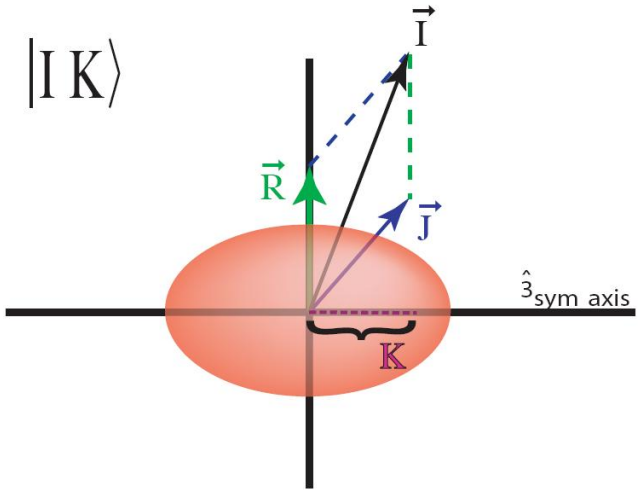

Figure 3: The body-frame representation of angular momentum states for the rotor model.

This decouples the internal degrees of freedom from those of the collective motion. Strongly-deformed even-even nuclei display these characteristics. The rotor model Hamiltonian takes the form

$$\hat{H} = A\hat{I}^2 + F\hat{I}_3^2, \tag{11}$$

and is diagonal in the basis $|IK\rangle$, with energy eigenvalues

$$E(I,K) = AI(I+1) + FK^2. \tag{12}$$

Even-even nuclei have a 0^+ ground state, and excited integer spin states. This results in two different groups of excited states, the $K^\pi = 0^+$ ground band and a series of excited bands with $K^\pi = 2, 4, 6, ...$ where K represents the spin projection on the body frame symmetry axis. Due to reflection symmetry of the nuclear shape, the $K^\pi = 0^+$ ground-band spins are $0, 2, 4, 6, ...$

2.2.2 The Triaxial Rotor

The triaxial rotor model was introduced by Davydov and Filippov [16]. The general Hamiltonian of a triaxial rotor [19] is

$$H = A_1\hat{I}_1^2 + A_2\hat{I}_2^2 + A_3\hat{I}_3^2, \tag{13}$$

where $A_1 = \frac{\hbar^2}{2g_1}$, etc., and g_1, etc., are the components of the inertia tensor in the principal axes frame. Then, defining

$$0 < A = \frac{1}{2}(A_1 + A_2), \quad 0 < F = A_3 - A, \quad 0 > G = \frac{1}{4}(A_1 - A_2), \tag{14}$$

the Hamiltonian can be rewritten in the form

$$\hat{H} = A\bar{I}^2 + F\bar{I}_3^2 + G(\bar{I}_+^2 + \bar{I}_-^2). \tag{15}$$

Further defining $\hat{H} = \hat{H}_0 + \hat{H}_1$ as

$$\hat{H}_0 = A\bar{I}^2 + F\bar{I}_3^2, \qquad \hat{H}_1 = G(\bar{I}_+^2 + \bar{I}_-^2), \tag{16}$$

$$\langle IK|\hat{H}_0|IK\rangle = AI(I+1) + FK^2, \tag{17}$$

$$\langle I, K \pm 2|\hat{H}_1|IK\rangle = G\sqrt{(I \mp K)(I \pm K + 1)(I \mp K - 1)(I \pm K + 2)}, \tag{18}$$

i.e., H_0 possesses diagonal elements, and H_1 has off-diagonal, $\Delta K = 2$ mixing elements.

2.3 The Nilsson Model

The Nilsson model [15] is a representation of deformed nuclei which describes independent nucleon motion in a deformed potential. This model uses an anisotropic harmonic oscillator with an added term, Dl^2, to flatten out the center of the nuclear potential. This effectively shifts the levels with higher l values to lower energy for $D < 0$. The Nilsson Hamiltonian is

$$H_{\text{Nil}} = \frac{p^2}{2m} + \frac{m}{2}(w_x^2 x^2 + w_y^2 y^2 + w_z^2 z^2) + C\vec{l} \cdot \vec{s} + Dl^2. \tag{19}$$

Nuclei are generally axially symmetric, this means the oscillator frequencies perpendicular to the symmetry axis are equal, i.e.,

$$w_x = w_y \equiv w_\perp \neq w_z. \tag{20}$$

Nuclear matter is also incompressible. This leads to volume conservation which constrains the values of $w_\perp$,w_z to the form

$$w_x = w_y \equiv w_\perp = w_o e^{\frac{\epsilon_2}{3}} \tag{21}$$

and

$$w_z = w_o e^{\frac{-2\epsilon_2}{3}}, \tag{22}$$

where the sign of the deformation parameter, $\epsilon_2 < 0$, results in an oblate shape and $\epsilon_2 > 0$ results in a prolate shape. The potential is then written as

$$V = \frac{1}{2} m w_o^2 r^2 - \beta_o m w_o^2 r^2 Y_{20}(\theta, \phi). \tag{23}$$

This allows the Hamiltonian to be diagonalized by fixing the parameters, $C, D, w_o, \epsilon_2, (\beta_o = -\frac{4}{3}\sqrt{\frac{\pi}{5}}\epsilon_2)$ and finding the eigenvalues and eigenvectors. Single-particle states and mean-square radii in nearby spherical nuclei fix C, D and w_o; β_o is fixed using quadrupole moments. This leads to two possible bases.

When ϵ_2 goes to 0 the states reduce to a spherical basis, defined by the Hamiltonian

$$H = \frac{p^2}{2m} + \frac{m}{2} w_o^2 r^2 + Cl \cdot s + Dl^2 + \beta_o m w_o^2 r^2 Y_{20}(\theta, \phi), \tag{24}$$

with the Y_{20} term as a perturbation, i.e., the approximate energy eigenstates are

$$|Nlj\Omega\rangle, \tag{25}$$

where N is the number of oscillator quanta, l is the single-particle angular momentum, j is the single-particle total angular momentum, and $\Omega = m_j$ is the projection of j=l+s along the symmetry axis.

When ϵ_2 goes to ∞, the states reduce to the asymptotic basis, defined by the Hamiltonian

$$H = (\frac{p_x^2 + p_y^2}{2m} + \frac{m}{2}w_\perp^2(x^2 + y^2) + \frac{p_z^2}{2m} + \frac{m}{2}w_z^2 z^2 + C\vec{l}\cdot\vec{s} + Dl^2), \tag{26}$$

with the $\vec{l}\cdot\vec{s}$ and l^2 terms as perturbations. The approximate energy eigenstates for this Hamiltonian are

$$|Nn_z\Lambda\Sigma\rangle, \tag{27}$$

where n_z is the number of oscillator quanta along the symmetry axis, N the total number of oscillator quanta, Λ is the component of angular momentum along the symmetry axis, and Σ the projection of the intrinsic spin along the symmetry axis ($\Omega = \Lambda + \Sigma$).

2.4 The Pairing Force Model

Nucleons are not independent particles, they are interacting fermions which have a tendency to pair off. Identical nucleons in $|j, m_j\rangle$ and $|j, -m_j\rangle$ states form a paired configuration that couples to $J = 0$. This mechanism effectively lowers the ground-state energy, producing a pairing gap. To describe the nuclear properties introduced by this pairing mechanism, we must add an additional potential of the form

$$V_{\text{pair}} = V^{\pi\pi} + V^{\nu\nu}, \tag{28}$$

where π denotes protons and ν denotes neutrons, respectively, and is only applicable when considering like-nucleon pairing.

The pairing model can be formulated using the Hamiltonian

$$H_{\text{pair}} = \sum_j \epsilon_j a_j^\dagger a_j - G \sum_{jk} a_k^\dagger a_{\bar{k}}^\dagger a_{\bar{j}} a_j, \tag{29}$$

where $a_j^\dagger(a_j)$ creates (annihilates) a nucleon in state $|j\rangle$ and $a_{\bar{j}}^\dagger(a_{\bar{j}})$ creates (annihilates) a nucleon in a time-reversed state $|\bar{j}\rangle$. The term $\sum_j \epsilon_j a_j^\dagger a_j$ is the energy contribution from single-particle motion, and $G\sum_{jk} a_k^\dagger a_{\bar{k}}^\dagger a_{\bar{j}} a_j$ describes the pairing interaction.

The structure of a paired state takes the form

$$|Pair\rangle = \sum_i C_i |j_i^2\rangle_{J=0}. \tag{30}$$

Breaking one nucleon pair requires an energy of approximately 2 MeV. This explains the energy gap seen in doubly-even nuclei. In addition the state density below 2 MeV is considerably lower in doubly-even nuclei than it is in odd or odd-odd nuclei. This low level density facilitates elucidation of nuclear structure.

2.5 Pair Excitations across Shells

Excitation of neutrons or protons across closed shells leads to a unique type of excited state in nuclei termed an intruder state. The interactions between two protons or two neutrons has been introduced. The interaction between proton pairs and neutron pairs can be added to the interaction potential,

$$V_{pair} = V^{\pi\pi} + V^{\nu\nu} + V^{\pi\nu}. \tag{31}$$

The excitation of pairs across single-particle energy gaps are lowered in energy by $V^{\pi\nu}$. Near doubly-closed shells these intruder states are at ≈5 MeV above the ground state. However as more valence pairs of nucleons are added to the system, these intruder states, by the midshell region, are as low as 2 MeV above the ground state.

A similar but less dramatic effect is observed for subshells. Particularly of interest in this study is the closed subshell of protons at $Z = 64$. As the neutron pair number is increased in the region from $^{150}_{60}$Nd to $^{160}_{70}$Yb, a sudden onset of deformation occurs. This is most dramatic at $^{154}_{64}$Gd [18] in the valley of β-stable nuclei. A goal of the present study is to investigate this deformation in $N = 90$ far from stability. The $N = 90$ nuclei have long been a challenge for theoretical modeling. It has been shown by Kulp et al. [18] that two different coexisting shapes, with mixing, are able to explain the sudden onset of deformation seen in ^{154}Gd. The sudden change in nuclear shape results when the more deformed (subshell) intruder state becomes the ground state. As one moves away from the closed subshell at $Z = 64$, to $^{160}_{70}$Yb, the subshell influence is observed to weaken.

2.6 Two-State Mixing

States with the same spin and parity can often occur sufficiently close in energy that two-state mixing results. Consider two states, $|\phi_1\rangle$ and $|\phi_2\rangle$, from different bands having the same parity and spin. Now perturbing this system with a phenomenological interaction potential V, we introduce the observed states

$$|\psi_1\rangle = \alpha|\phi_1\rangle - \beta|\phi_2\rangle, \qquad |\psi_2\rangle = \beta|\phi_1\rangle + \alpha|\phi_2\rangle, \tag{32}$$

where $|\psi_1\rangle$ and $|\psi_2\rangle$ are the perturbed wave functions for bands 1 and 2, and α and β are the amplitudes of the major and minor components respectively, with $\alpha \geq \beta$ and $\alpha^2 + \beta^2 = 1$.

The two unperturbed energy levels, E_1 and E_2, after diagonalizing the interaction matrix, lead to

$$\lambda_{1,2} = \bar{E} \mp \sqrt{\frac{1}{4}\epsilon^2 + V^2}, \tag{33}$$

where $\bar{E} = \frac{E_1+E_2}{2}$, and $\epsilon = |E_2 - E_1|$. Expressions for the coefficients in $|\psi_1\rangle$, $|\psi_2\rangle$ are found by substituting the solution for E into the state equation. The results are

$$\alpha^2 = \frac{V^2}{V^2 + (\lambda_1 - E_1)^2} \quad , \qquad \beta^2 = [1 - \alpha^2]. \tag{34}$$

This demonstrates how an interaction potential causes two energy levels to repel. Leading to a lowering in energy of the lower initial state, and a raising in energy of the higher initial state.

2.7 The N=90 nuclei

The $N = 90$ isotones offer one of the biggest challenges to collective models. These nuclei lie on the edge of a rapid change from spherical to deformed shapes, with a variety of coexisting structures present. Collecting very detailed spectroscopic information will allow us to elucidate the nuclear structure involved in this deformation. Beyond $^{152}_{62}$Sm and $^{154}_{64}$Gd very little detailed information is available. The present study of $^{160}_{70}$Yb aims to uncover the structural features of this nucleus in as great a detail as possible. These features will, in turn, further reveal the systematic changes in the collective structure of the $N = 90$ isotones.

When one compares the $N = 90$ isotones, the structure of the ground bands are remarkably similar. The energy spacings are nearly identical, the heads of the β bands are at nearly the same energy and the band-head energies of the γ-band are changing in a systematic way. The nucleus $^{160}_{70}$Yb lies further from β stability than the well studied $N = 90$ nuclei. Figure 4 shows the systematics of these transitional nuclei.

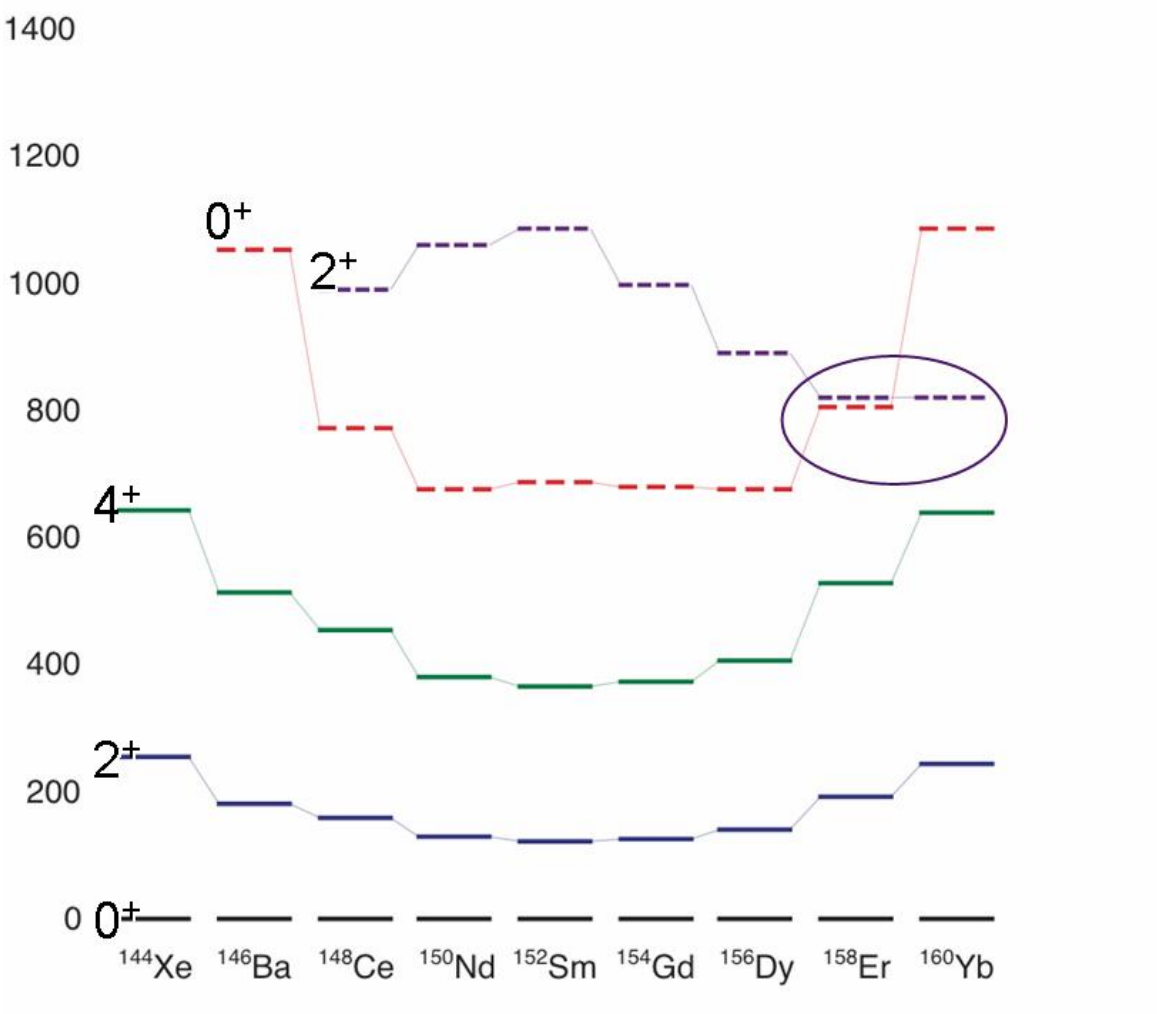

Figure 4: The low-energy positive-parity structure, up to $I = 4^+$, for the $N = 90$ nuclei, including the location of the 0^+_β and 2^+_γ band heads.

Figure 4 displays information about the $N = 90$ nuclei. The nuclei near stability, are all very similar in low-energy band structure. Note the crossing of the bandhead energies from $^{158}_{68}$Er to $^{160}_{70}$Yb.

Strong support for the concept of rotational collective motion comes from the widespread observation of large electric quadrupole moments in nuclei [11]. This was the basis for the Bohr collective model [12], and was thoroughly developed by A. Bohr and B. Mottelson [15].

CHAPTER III

EXPERIMENTAL

3.1 Introduction

The present study is based on data obtained at TRIUMF in Vancouver, Canada using the ISAC facility. A target of high-purity tantalum ($^{181}_{73}$Ta) was bombarded with a 40 μA beam of 500 MeV protons. Spallation products from the bombardment recoiled into the ion source of the on-line isotope separator [18]. Beams of spallation products with $A = 160$ were delivered to the 8π/PACES spectroscopy station.

Figure 5 shows a schematic view of the spallation production of the isotopes relevant to the present study.

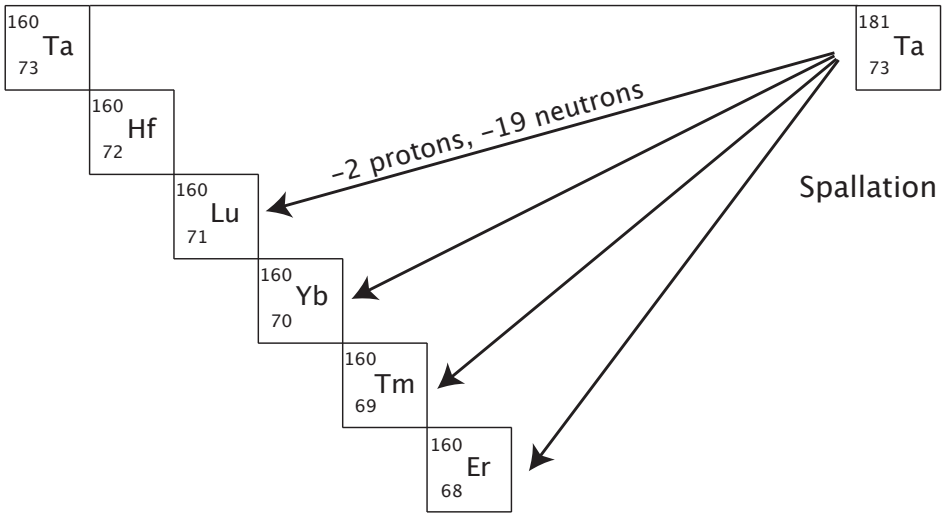

Figure 5: Spallation production of $A = 160$ isobars relevant to this experiment.

The production of ^{160}Lu required the loss of 2 protons and 19 neutrons from the target nucleus. The beam of spallation products after mass separation contained ^{160}Lu, ^{160}Yb, ^{160}Tm and ^{160}Er. Figure 6 shows some details of these $A = 160$ isobaric nuclei.

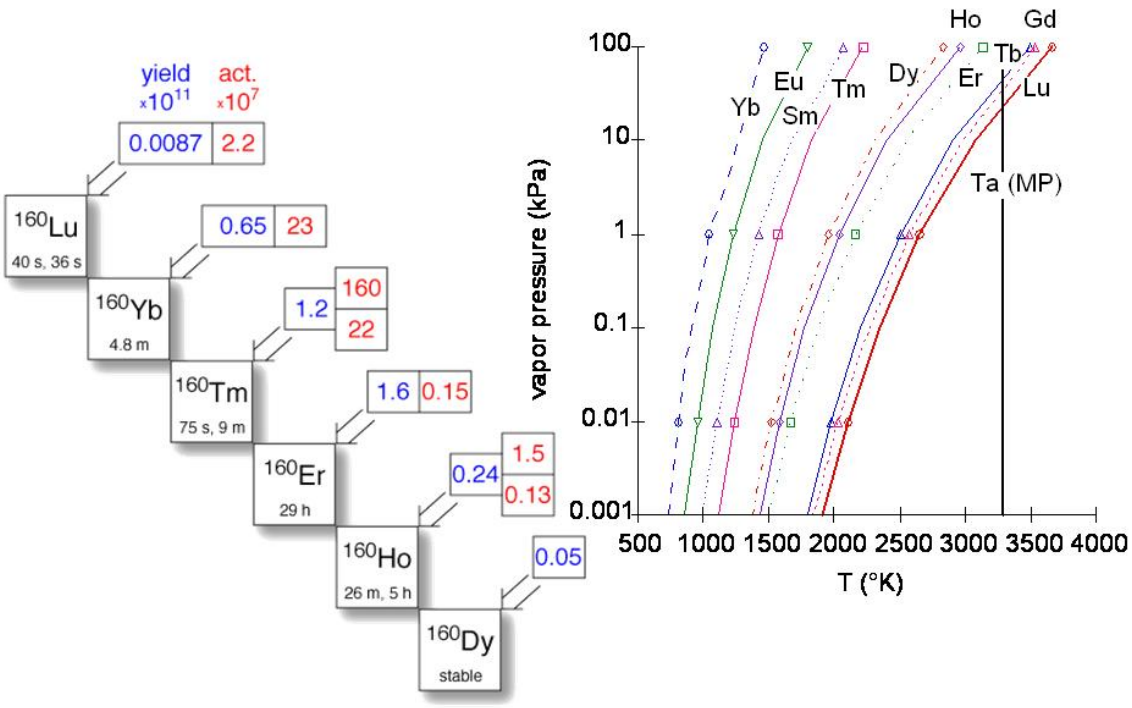

Figure 6: Yields of $A = 160$ isobars calculated using the code of Silberberg-Tsao [18]; and vapor pressures of the elements of interest. (See text for further details.)

Figure 6a shows the theoretical yields and activities of the mass 160 nuclei produced by the spallation reaction, highlighted in blue and red, respectively, above each mass 160 isobar produced. The activities of the lower Z isobar nuclei contribute many γ rays to the spectra in the present work. This study was directed at maximizing the production and collection of ^{160}Lu, however the other mass-separated products in the decay chain were much more abundant, as indicated by their large relative activities. Figure 6b is a temperature (K) vs. vapor pressure (kPa) graph for the nuclei observed in the present study. The operating temperature of the Ta target was maintained at $\approx$ 2500 K. This high temperature, while approaching the melting point of the Ta target foils, was marginally effective at vaporizing the ^{160}Lu spallation products. The collection of ^{160}Lu produced was hindered by the fraction that remained in the target.

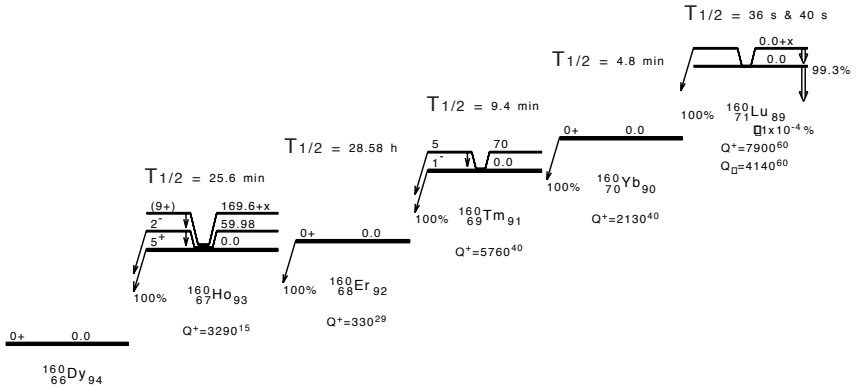

The A=160 β+/EC decay chain showing the decaying species relevant to the present investigation.

Figure 7: The β-decaying isomers observed in this $A = 160$ decay chain study. The level energies, decay energies, and Q^+ values are given in keV. The decaying states are labeled by their spins, parities, and half lives.

Figure 7 gives relevant nuclear decay properties for the nuclei involved in this study, viz. the decays of ^{160}Lu, ^{160}Yb and ^{160}Tm. One should note the difference in Q values of the decays involved, as well as the multiple β-decaying isomers present. The spallation process generates nuclei in a variety of spin states, which lead to high- and low-spin population of bands in the daughter nuclei.

3.2 Moving tape collector

The radioactivity for this experiment was collected on the moving tape system shown in Figure 8. This system permitted an emphasis to be placed on the short-lived decay of ^{160}Lu to ^{160}Yb. The tape was moved every 43 seconds to maximize the activity of the two β-decaying isomers with half lives of 36 s and 40 s. Longer-lived activities were transported away so that the source in front of the detectors was replaced frequently with a maximum ratio of short-lived to long-lived decay. High-statistics spectra were also acquired for the ^{160}Yb (4.8 min) decay to ^{160}Tm and ^{160}Tm (9.4 min, and 74.5 sec) decay to ^{160}Er, with no optimization by tape moves.

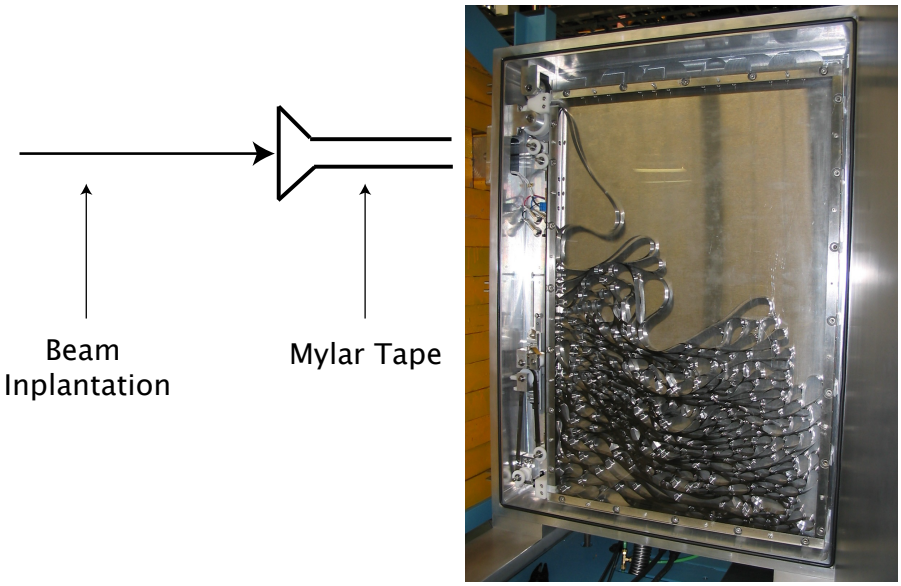

Figure 8: The moving tape system.

The species ^{160}Lu will comprise the smallest fraction of the $A = 160$ mass-separated beam. The counting time in the ^{160}Lu study was ≈100 s, which was to optimize the acquisition of ^{160}Lu ($T_{1/2}$ = 36 and 40 s). A 1000 s counting time was employed to characterize the longer-lived decays of ^{160}Yb to ^{160}Tm and ^{160}Tm to ^{160}Er. As noted, the activities from the decay of these lower Z isobars led to high-statistics data for these longer-lived species.

3.3 The 8π γ-ray spectrometer

The data from this study were collected using the 8π spectrometer. Details of the detector array are outlined here, as well as the relevant details of the facility at TRIUMF. The 8π spectrometer represents a vast improvement in γ-ray collection capability over the systems that were previously available for the study of ^{160}Yb. One advantage that this system offers is a much higher detection efficiency (1.5 percent absolute γ-ray efficiency at 1.33 MeV), especially needed to observe weak transitions in coincidence spectra.

Figure 9 shows the detector arrangement of the 8π, which is used for γ ray energy collection in the present study.

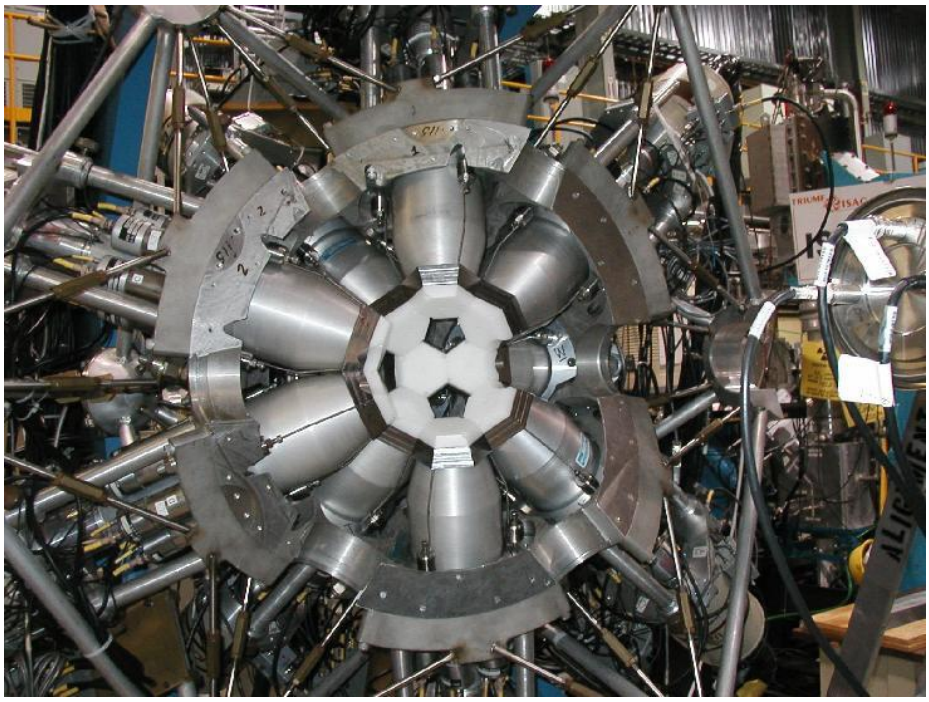

Figure 9: The 8π spectrometer (open view).

At the heart of the 8π spectrometer is a close-packed array of 20 High Purity Germanium (HPGe) detectors, positioned in order to minimize angular correlation distortion of coincidence intensities. The HPGe detectors are surrounded by bismuth germinate (BGO) Compton suppression shields. Compton suppression is necessary in order to reject events where the total γ ray energy is not deposited in a Ge detector. If a photon Compton scatters out of the detector, the BGO array detects this. Such events are vetoed in order to produce spectra relatively free of Compton artifacts.

The relative γ-ray photopeak detection efficiency for the 8π array is shown in Figure 10. It was determined using the following procedure. Coincidence gates on γ rays feeding the 6^+ level at 765 keV in the decay of ^{160}Tm to ^{160}Er show the sequential cascade, $6^+ - 4^+ - 2^+ - 0^+$, of the 376, 264 and 126 keV γ rays. Fitting the areas of these transitions with Gaussian peaks allows the deduction of relative efficiency calibration points at 126, 264 and 376 keV. This establishes the most important part of the efficiency curve.

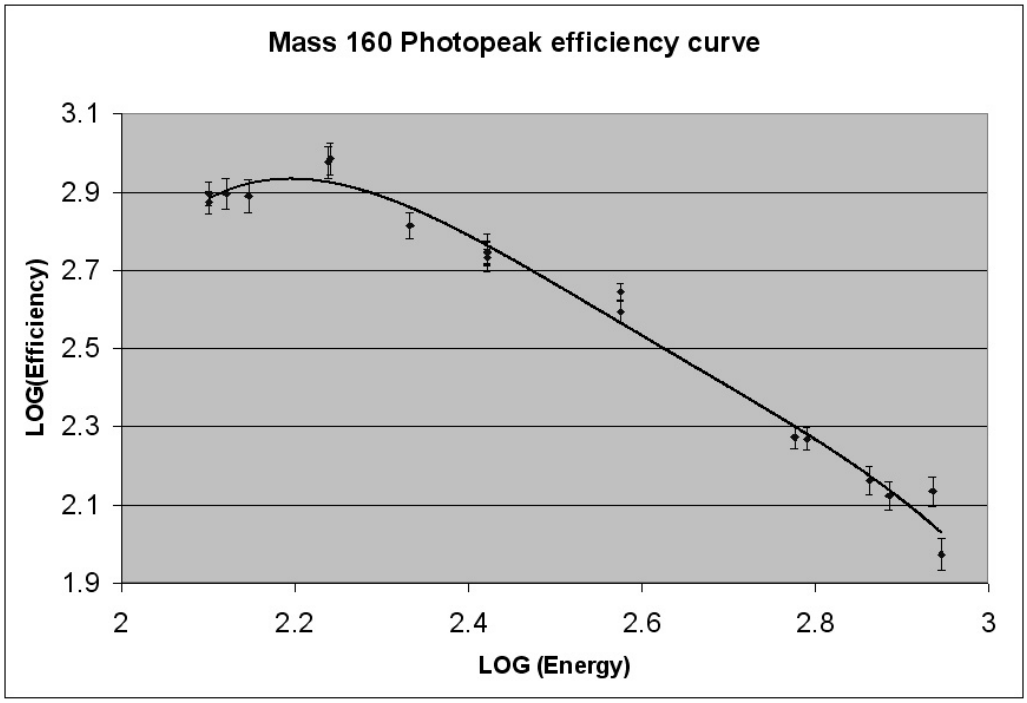

Figure 10: The photopeak detection efficiency for the 8π array.

The next iteration made to create the photopeak efficiency curve was to normalize other coincidence gates to a reference point and add information about higher energy regions. A reference point is established at 264 keV $I_\gamma \equiv 100$, and coincidence gates on the 126, 264 and 376 keV transitions give relative efficiency points up to 1000 keV. Figure 10 displays the fourth-order polynomial fit for the photopeak efficiency curve used for analysis in the present work. An uncertainty based on the fitting of the area is determined.

3.4 The Pentagonal Array for Conversion Electron Spectroscopy

The PACES system developed by E. Zganjar at LSU [18], is a detector array composed of 5 Si(Li) detectors, each 5mm thick, and 250 mm^2 in area, symmetrically placed as shown in Figure 11. Conversion electron spectroscopy offers an additional source of coincidence information for the present study. One advantage of combining γ-ray information with conversion electron information is the detection efficiency difference between the two systems. The Si(Li) detector system is sensitive down to about 15 keV, providing accurate coincidence information on many low-energy transitions not observable by the Ge detector array.

Information about the multipolarity of a nuclear transition is also obtained from conversion electron spectroscopy. Atomic electrons have a finite probability of being inside the nucleus. The internal conversion process results in the energy of the excited nucleus being imparted to an electron. Conversion electrons for a single nuclear transition are observed at different energies depending on the binding energy of the electron shell involved. The internal conversion process creates an electron shell vacancy which is filled when a higher-shell electron undergoes a transition, and the energy may result in an x-ray. The energy of the electrons is collected by the PACES detector array and analysis of these electron peaks allows the detailing of levels with spin and parity assignments.

Figure 11 displays the PACES array as it was situated within the 8π spectrometer for the present study.

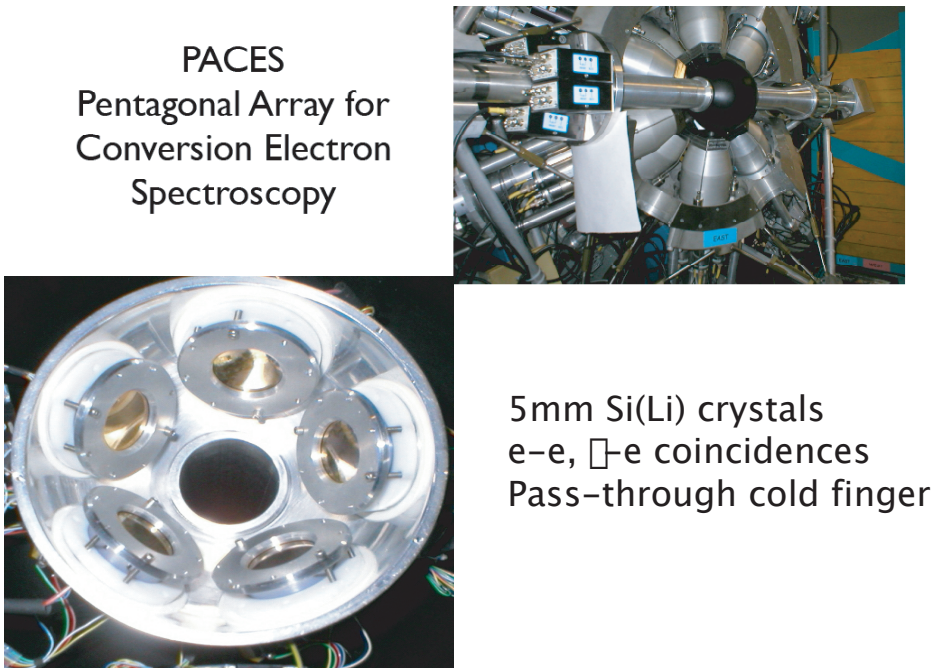

Figure 11: The PACES detector array

The PACES system fits inside of the 8π and sits upstream of the beamline that passes through its middle. The detectors are cooled to liquid nitrogen temperature to reduce noise. These 5 detectors provide γ-electron coincidences as well as electron-electron coincidences for the present analysis.

The probability of internal conversion changes with the energy of a transition. Low-energy transitions are more likely to convert internally than are high-energy transitions.

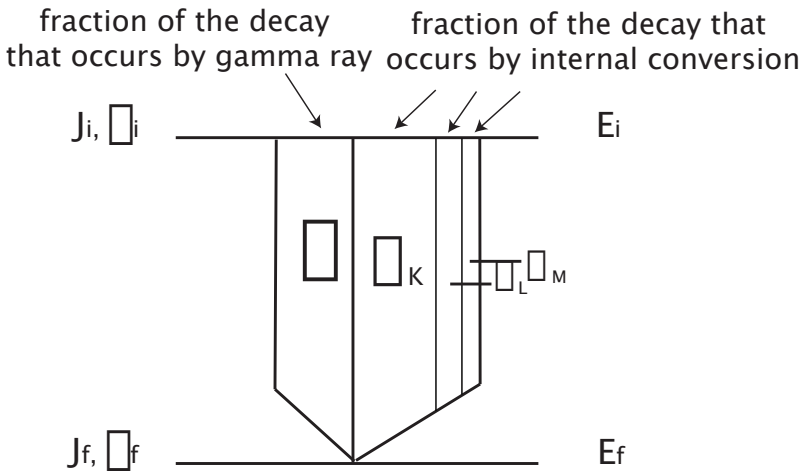

Figure 12: The details of the γ ray and conversion electrons involved in a nuclear transition.

Figure 12 shows the details of a nuclear transition. These notations are used throughout this narrative for describing nuclear transitions. These transitions are classified by an intensity, and are assigned a percentage of internal conversion (α). The coefficient α is further broken down by classification of the electron orbital involved in the transition: α_K, α_{L_1}, α_{L_2} etc. Fractional values will be calculated for the transitions observed in these decays. The details and notations for classifying nuclear transitions are as tabulated by ENSDF (Evaluated Nuclear Structure Data File).

Various transitions shown throughout this work include, E0 (electric monopole), E1 (electric dipole), E2 (electric quadrupole) and M1 (magnetic dipole) transitions. Particular multipolarity assignments will be shown with supporting conversion electron data. The multipolarity of each γ ray is used to infer spin and parity assignments for energy levels

involved in the transition.

Table 1: Types of transitions

	Spin Change	Parity Change
E0	0	*no*
E1	1	*yes*
E2	2	*no*
M1	1	*yes*

Table 1 displays the common multipolarities observed for nuclear transitions in the present study. Assignments for new and rearranged levels will be made where supporting conversion electron data are available.

3.5 Data flow and event reconstruction

The active spot of mylar tape sits at the center of the array (8π + PACES). The data stream is started when the pre-amplifier receives a signal pulse from the detector array. There is both timing and energy information for each signal. The ADC (analog to digital converter) passes a header along with the energy information to the MIDAS system. The TDC (time to digital converter) passes a header along with timing information to the MIDAS system as well. The MIDAS system combines the pair of signals with a master clock signal and exports this information. The MIDAS data includes a header and main clock tag, along with the ADC and TDC information bundled together. This study was assisted with computer code written by G. Demand. (U. of Geulph) which translated the MIDAS data into coincidence matrices.

The present study characterized the system at the time of the run to use a coincidence window of 100 μ seconds. This is the maximum allowable timing difference between signal pulses from transitions in coincidence. The matrices assembled for this study include, γ rays in coincidence with γ rays, conversion electrons in coincidence with γ rays, and γ rays in coincidence with conversion electrons.

These matrices have been analyzed using the spectroscopy software written by D. Radford (Oak Ridge) called GF3. This software allows the generation of coincidence spectra with background subtraction. Coincidence spectra with transition information relevant to the narrative will be shown.

CHAPTER IV

RESULTS

4.1 Previous studies of the $A = 160$ isobars

The decay of ^{160}Lu to ^{160}Yb has been studied by Auer et al. [3] and Gelletly et al. [5]. Two β-decaying isomers have been proposed in ^{160}Lu. The decay of ^{160}Yb to ^{160}Tm has been studied by Schilling et al. [6]. The decay of ^{160}Tm to ^{160}Er has been studied by Strusny et al. [7], Bykov et al. [8] and Singh et al. [9]. Two β-decaying isomers have been proposed in ^{160}Tm.

The nucleus ^{160}Yb has also been studied using the ^{159}Tb (^{6}Li,5n) reaction (in beam) by Dusling [10] . This study observes high-spin states, and the only overlap with the present work is for the ground-state band to spin $J^{\pi} = 6^{+}$.

4.1.1 The β^+ decay of ^{160}Lu to ^{160}Yb

Figure 13 is the ENSDF (Evaluated Nuclear Structure Data File) decay scheme for the decay of ^{160}Lu to ^{160}Yb, displaying information known about this decay. The spins of the β decaying states are unknown. The relative intensities for the decay branches from the two β-decaying states are also unknown.

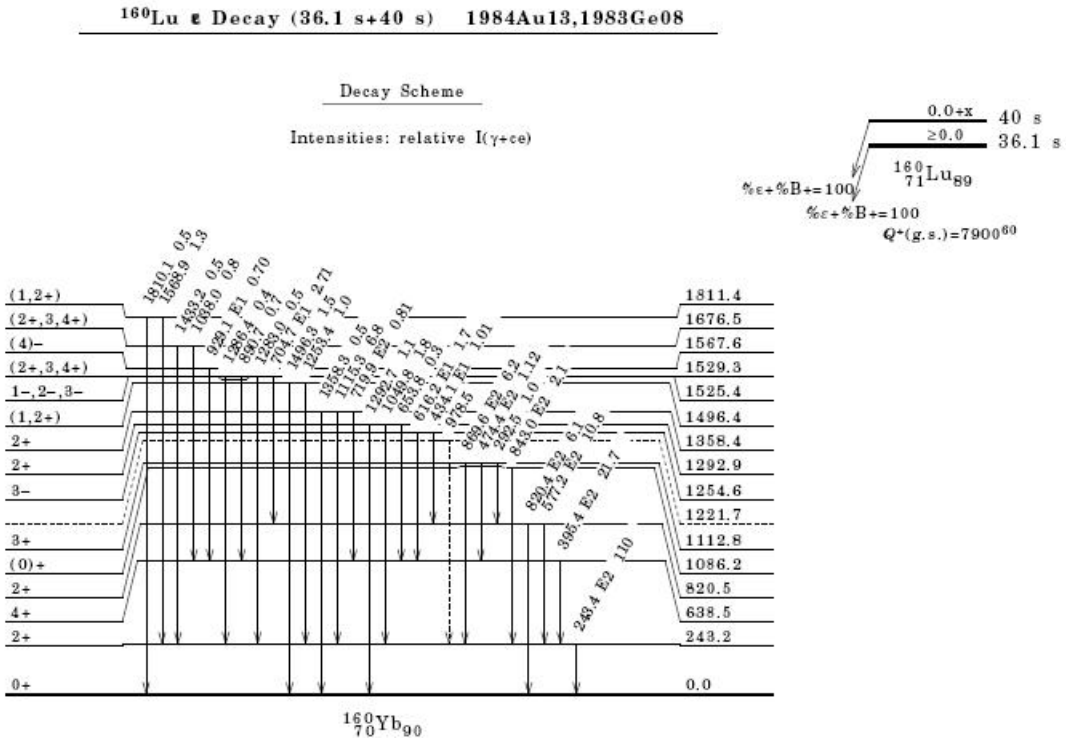

Figure 13: ENSDF Decay scheme for ^{160}Lu to ^{160}Yb.

4.1.2 The β^+ decay of ^{160}Yb to ^{160}Tm

Figure 14 shows the ENSDF decay scheme for the decay of ^{160}Yb to ^{160}Tm, i.e., of the 0^+ β-decaying ^{160}Yb ground state.

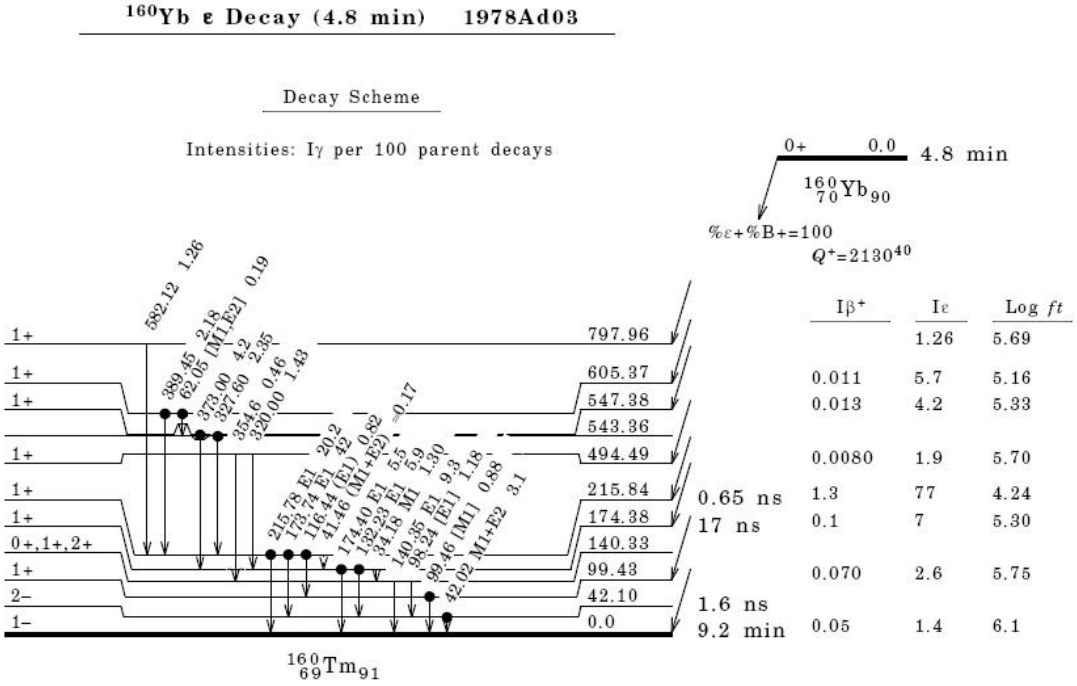

Figure 14: ENSDF Decay scheme for ^{160}Yb to ^{160}Tm

4.1.3 The β^+ decay of ^{160}Tm to ^{160}Er

Figure 15 shows the ENSDF decay scheme for the 1^- β-decaying isomer of ^{160}Tm to ^{160}Er.

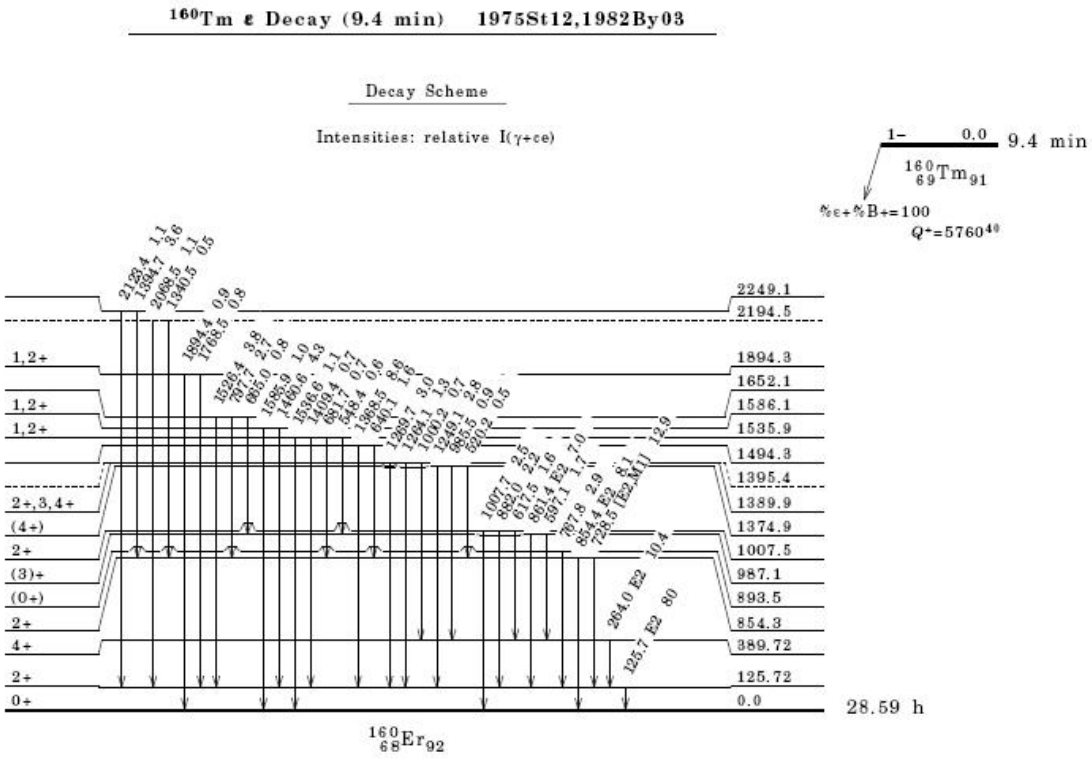

Figure 15: ENSDF decay scheme for ^{160}Tm (9.4 min) to ^{160}Er

4.1.4 The β^+ decaying isomer of ^{160}Tm to ^{160}Er

Figure 16 shows the ENSDF decay scheme for the spin-5 β-decaying isomer of ^{160}Tm to ^{160}Er.

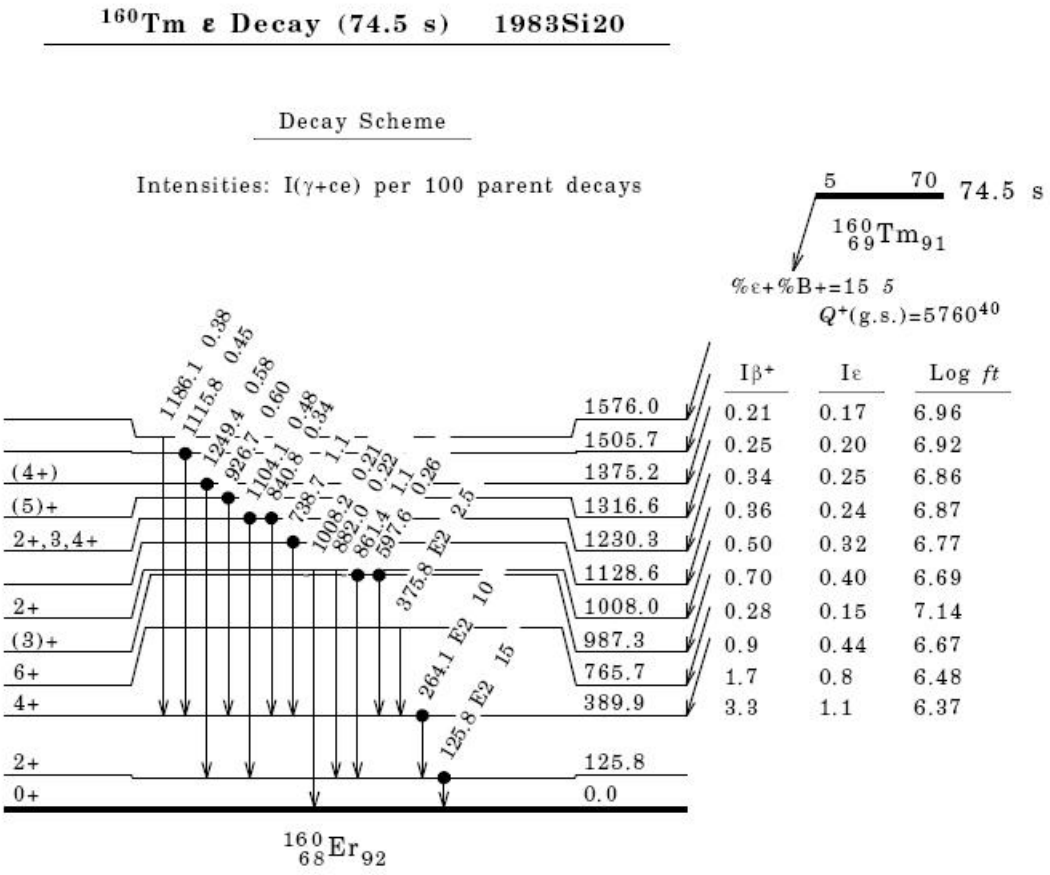

Figure 16: ENSDF decay scheme for ^{160}Tm (74.5) s to ^{160}Er.

4.2 Spectroscopy of $^{160}_{70}$Yb from the decay of $^{160}_{71}$Lu

Support for the identification of γ-rays in the decay of ^{160}Lu is obtained in the present work from a combination of spectra. A selected region of the projection of the γ-γ coincidence spectrum is shown in Figure 17. This projection is matched against a γ-ray coincidence gate on the annihilation line at 511 keV. A high Q value increases the probability of positron emission relative to electron capture. This results in the 511 keV, annihilation line being dominated by contributions from the high-Q decays. The coincidence gate on the 511 keV peak emphasizes the γ rays in ^{160}Yb, because the decay of ^{160}Lu to ^{160}Yb has a Q value of 7900 keV.

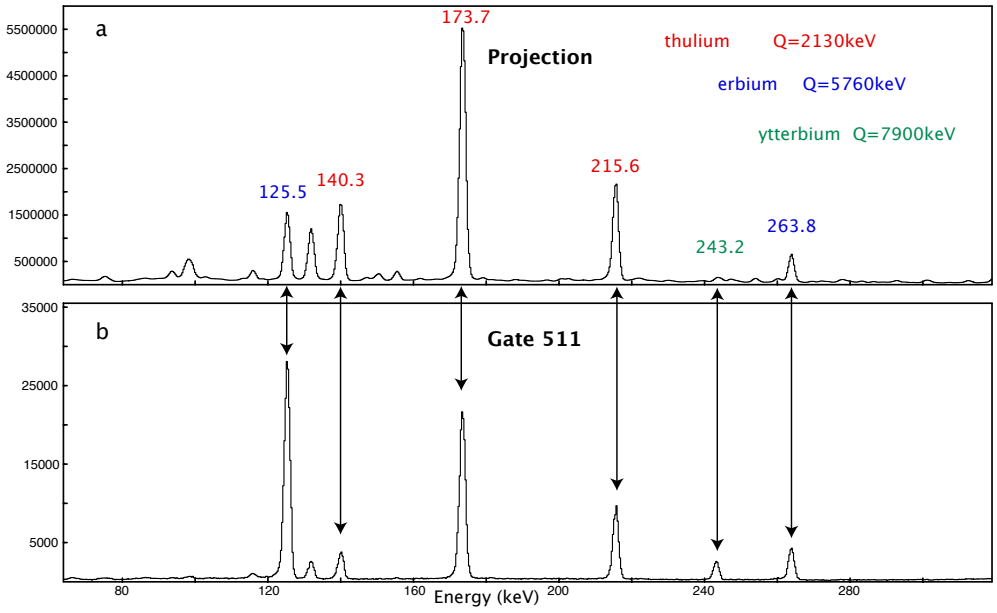

Figure 17: Coincidence gate on the 511 keV annihilation line matched with the γ-γ coincidence projection.

In Figure 17a the strongest transitions in each nucleus of the $A = 160$ decay chain are highlighted. In Figure 17b the same peaks are seen in different proportions due to the difference in Q value of the decay. The displayed Q values give an indication from which nuclei γ rays will be emphasized in the 511 keV gate.

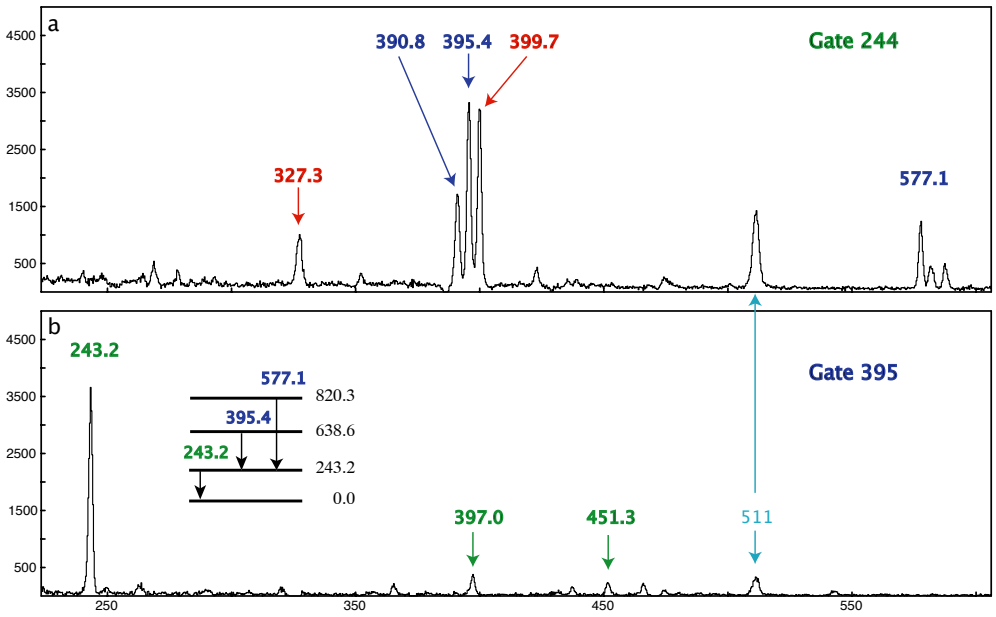

Figure 18: Coincidence gate on the 243 keV γ ray, along with the 395 keV γ ray.

Figure 18a displays γ-rays (not all from ^{160}Lu) in coincidence with the 243 keV peak. The energy window used for the coincidence gate on the 243 keV peak included the 243 keV 2_g^+ to 0_g^+ transition, the strongest γ ray in this decay, as well as γ rays from the decays of the other $A = 160$ isobars. This is because many (closely-spaced) lines occur in the wide energy window used in this gate. Figure 18b shows γ-rays in coincidence with the 395 keV 4_g^+ to 2_g^+ transition, the second strongest γ ray in the ^{160}Lu decay.

The following technique was used to produce γ-ray coincidence spectra for the 243 keV transition where γ rays from the decay of $A = 160$ isobars have been removed. Closely-spaced lines are resolved by using a running gate. A running gate uses a narrow energy window which is advanced step-wise in energy. Figure 19 is an example of a running gate.

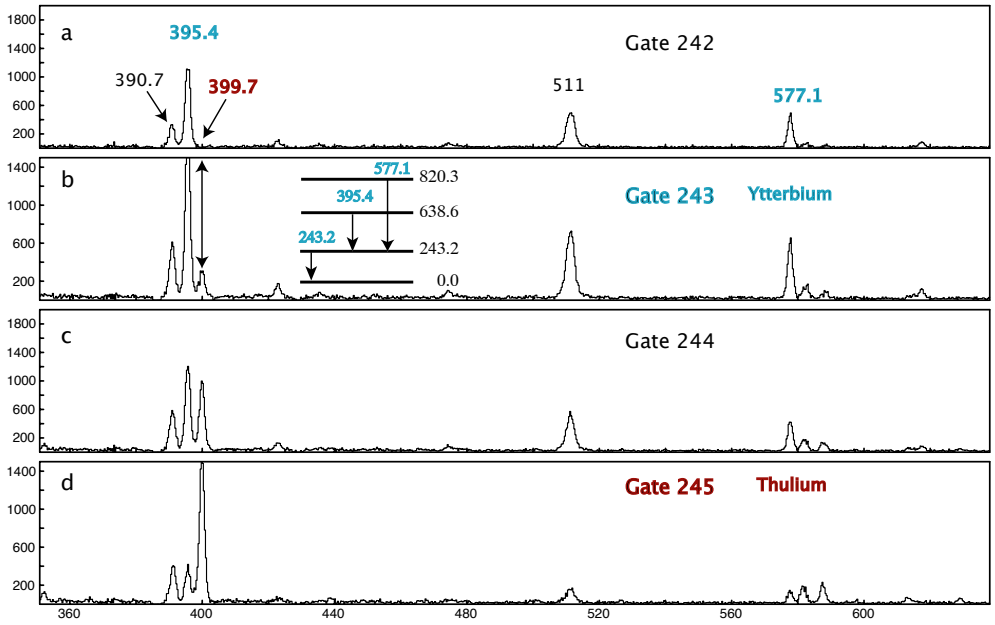

Figure 19: Running coincidence gate on the 243 keV peak aimed at identifying transitions in the decay of ^{160}Lu to ^{160}Yb. The inset decay scheme displays the 577 keV γ-ray transition from the 820 keV 2^+ level.

Figure 19 displays the same energy range as Figure 18, but now the 243 keV coincidence gate is split into 4 smaller energy windows of 1 keV width. The smaller energy windows used here show coincidence information in finer detail. Figures 19a,b show the 395 and 577 keV γ rays both in coincidence with the 243 keV γ ray. Figures 19c,d show the 399 keV γ ray in coincidence with a 245 keV γ ray from the decay of ^{160}Yb to ^{160}Tm. The 390 keV γ ray is seen in each coincidence window and does not rapidly diminish by Figure 19d such as observed for the 395 and 577 keV transitions, therefore it is not assigned to the decay of ^{160}Lu.

Table 2 lists the energies and intensities of γ rays assigned to the decay of ^{160}Lu to ^{160}Yb. Each of these assignments has been checked to ensure that γ rays from the decays of other

$A = 160$ isobars are not being assigned to the decay of ^{160}Lu.

Table 2: Transitions in Yb

$\mathbf{E}_\gamma$		$\mathbf{I}_\gamma$		**Levels**	
Present study	**Auer et al.**	**Present study**	**Auer et al.**	E_i	E_f
243.2	243.4	100.0	100.0	243.2	0.0
292.0	292.5	0.3	1.0	1112.8	820.3
395.4	395.4	20.6	21.0	638.5	243.2
435.0	434.1	0.5	1.0	1254.6	820.3
474.1	474.4	1.0	1.1	1112.8	638.5
577.1	577.2	13.1	10.7	820.5	243.2
616.8	616.2	3.3	1.7	1254.6	638.5
654.1	653.8	1.1	0.3	1292.9	638.5
704.7	704.7	2.4	2.7	1525.4	820.3
719.8	719.9	1.5	0.8	1358.4	638.5
820.0	820.4	8.9	6.1	820.5	0.0
844.2	843.0	1.6	2.1	1086.2	243.2
869.7	869.6	10.8	6.2	1112.8	243.2
890.7	890.7	1.1	0.7	1529.3	6.8.5
928.8	929.1	1.7	0.7	1567.6	638.5
977.9	978.5	1.6		1221.7	243.2
1037.6	1038.0	1.4	0.8	1676.5	638.5
1049.8	1049.8	2.1	1.8	1292.9	243.2
1056.4	1056.4	2.7		1694.9	638.5
1116.1	1115.3	14.4	6.8	1358.4	243.2
1117.4	1117.4	0.8		1811.4	638.4
1253.5	1253.4	0.7	1.0	1496.4	243.2
1282.9	1283.0	3.3	0.5	1525.4	243.2
1287.8	1286.4	1.9	0.4	1529.3	243.2

4.2.1 Excited states in ^{160}Yb

This study corroborates all 15 reported excited states in ^{160}Yb at 243, 638, 820, 1086, 1112, 1221, 1254, 1292, 1358, 1496, 1525, 1529, 1567, 1676 and 1811 keV and adds one additional one at 1694 keV. Figure 18 displays the spectra demonstrating the population of the excited states in ^{160}Yb.

The 243 keV level previously reported is fed by many transitions, including the 395 keV transition from the level at 638 keV and drained by the 243 keV transition to the ground state. The present study observed the 577, 843, 869, 978, 1049, 1115, 1253, 1283 and 1286 keV transitions feeding from the 820, 1086, 1112, 1221, 1358, 1292, 1358, 1496, 1525 and 1529 keV levels, respectively. Coincidence intensities are reported for these transitions using the previous 395 keV intensity as a normalization.

The 638 keV level previously reported is fed by several transitions including the 474 keV transition from the level at 1112 keV and drained by the 395 keV transition. This level has additional feeding observed from the 616, 653, 719, 890, 929, 1038, 1056 and 1117 keV transitions from the 1254, 1292, 1358, 1529, 1567, 1676, new 1694 and 1811 keV levels, respectively. Coincidence intensities are reported for these transitions using the previous 243 keV intensity as a normalization.

The previously reported level at 820 keV is fed by the 292, 434, 704 keV transitions from the levels at 1112, 1254 and 1525 keV. Coincidence intensities are reported for these transitions using the previous 243 keV intensity as a normalization. The information known about the structure of the excited states in ^{160}Yb will be summarized in the discussion.

4.3 Spectroscopy of $^{160}_{68}$Er from the decay of $^{160}_{69}$Tm

The production of ^{160}Tm by spallation leads to the β-decaying isomers, $T_{1/2} = 74.5$ s, $J = 5$ and $T_{1/2} = 9.4$ min, $J^{\pi} = 1^{-}$. The decay schemes deduced from previous studies are given in Figures 15 and 16, respectively. Table 3 compares the γ-ray intensities in the present study to the work of Strusny et al. [7], Bykov et al. [8] and Singh et al. [9].

The 100 second counting time used for this experiment maximized the activity of the spin-5 isomer. Spectra containing γ rays from the $J = 5$ decay are shown in Figure 20. The 6^{+} to 4^{+} transition, at 376 keV, is seen in coincidence with both the 4^{+} to 2^{+} and the 2^{+} to 0^{+} γ rays at 265 and 126 keV, respectively. The 376 keV transition is only populated by the $J = 5$ decay.

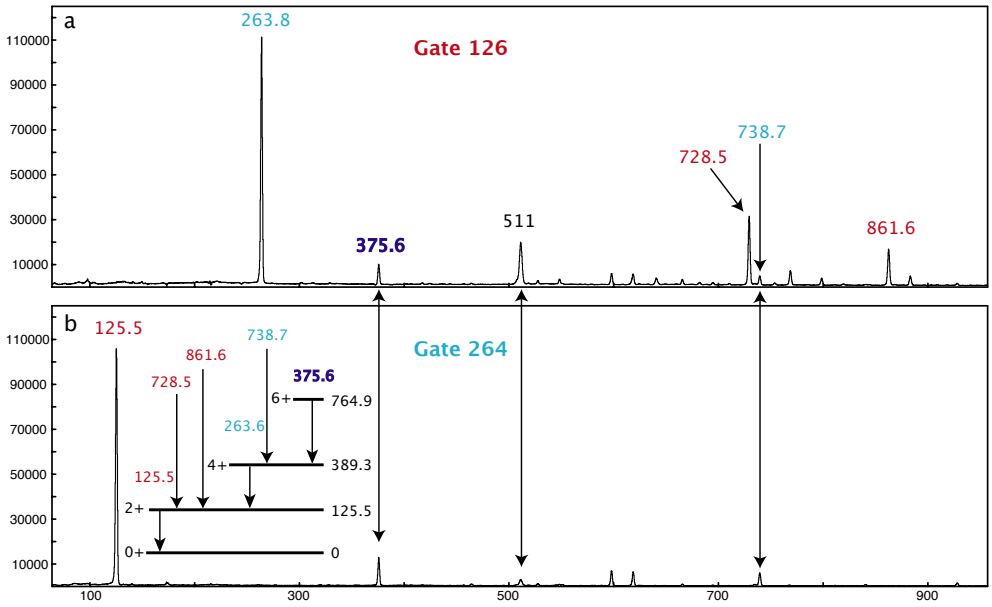

Figure 20: Coincidence gates on the 126 keV γ ray matched with the 264 keV γ ray feeding from above, as shown in the inset.

The 126 keV γ-ray coincidence gate shows many γ rays, including the 728, 738, and 861 keV. Figure 20a uses different colors to indicate which β-decaying isomer feeds the transitions corresponding to these γ rays. Figure 20b indicates the γ rays in coincidence with the 264 keV γ ray.

The level diagram (inset) displays basic spin and parity information and γ-ray transition locations. The 376 and 738 keV γ rays, observed in both coincidence gates, were identified by Singh et al. [9], as belonging to the $J = 5$ β-decaying isomer. The 728 and 861 keV γ rays were identified by Strusny et al. [7] and Bykov et al. [8] and assigned to the 1^- β-decaying isomer. Looking at the γ rays feeding the 6^+ level at 765 keV helps to elucidate the other energy levels populated in the spin-5 β-decaying isomer.

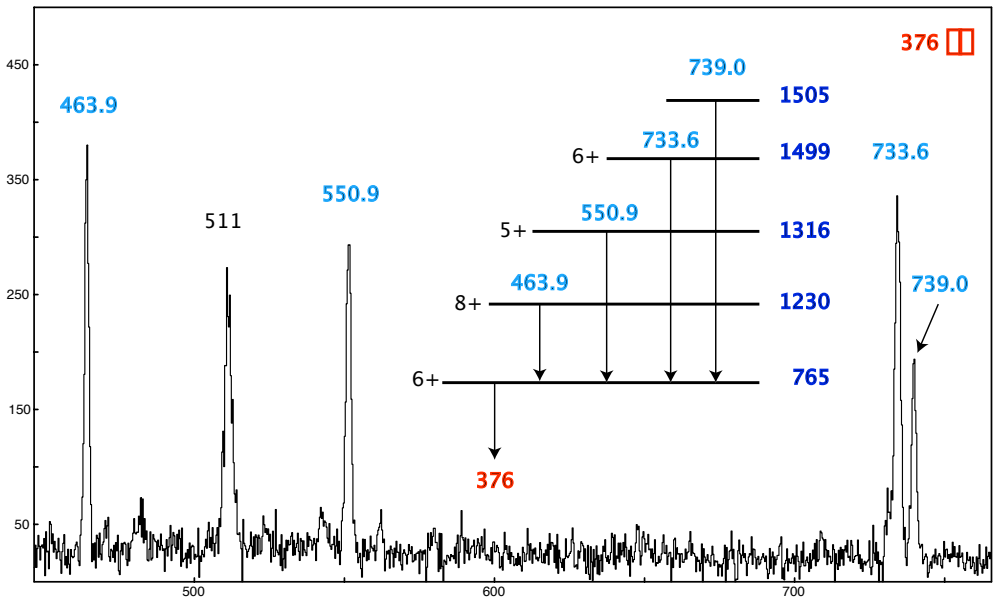

Figure 21: Transitions in coincidence with the 376 keV γ ray are fed only by the $J = 5$ β-decaying isomer of ^{160}Tm.

Figure 21 shows a coincidence gate on the 376 keV γ-ray, which is the 6^+ to 4^+ ground-band transition. This gate contains γ rays exclusively from the spin-5 decay of ^{160}Tm. The 464, 551, 733, and 739 keV γ rays are observed in coincidence with the 376 keV γ ray. The 464 keV γ ray is a transition from the 8^+ ground-band state at 1230 keV observed by Dusling et al. [10]. The 551 keV γ ray is a transition from the 5^+ level at 1316 keV, reported by Singh et. al [9]. The 733 keV γ ray is a transition from the 6^+ γ-band state at 1499 keV, identified by Dusling et al [10]. The 739 keV γ ray is a transition from the 1505 keV level, with no spin or parity assignment, seen by Singh et al. [9].

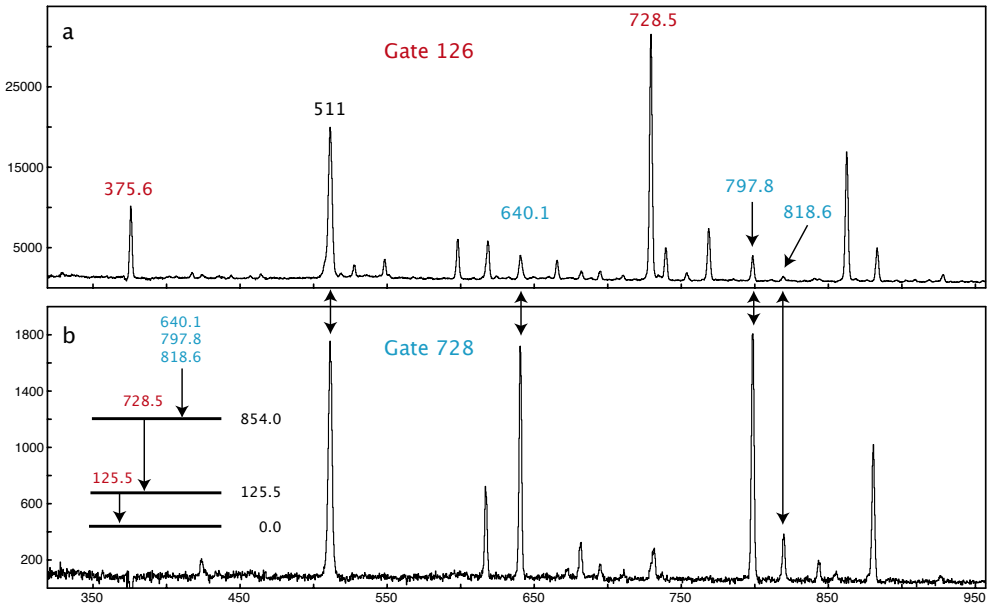

Figure 22: Coincidence gate on the 126 keV γ ray now matched with a coincidence gate on the 728 keV γ ray feeding from above.

Figure 22a shows a selected energy range for the γ rays observed in the 126 keV γ ray coincidence gate. It is shown again for comparison to display relative intensities of the γ rays observed. Figure 22b shows a coincidence gate on the 728 keV γ ray. The 728 keV γ ray is a transition from the 2^+ γ-band level at 854 keV. This allows inspection of the decay from the γ band.

The γ-ray transitions observed in Figure 22b are above the level at 854 keV. From higher energy levels in ^{160}Er one observes the 640, 798, and 818 keV γ rays. These γ rays are seen weakly in the 126 keV coincidence gate and are stronger in the 728 keV coincidence gate. The 640 and 798 keV γ rays are transitions from the 1494 and 1652 keV levels, respectively, with no assigned spin or parity information, observed by Strusny et al. [7] and Bykov et

al. [8]. The 818 keV γ ray is a transition from a level at 1672 keV, newly reported in the present work.

Intensity information for these inter- and intra-band transitions from levels in the γ band of ^{160}Er contribute to an analysis of its rotational characteristics. Comparing the strength of a γ ray with the spin change for these inter-band transitions will be the basis of producing a Mikhailov plot, which will be developed in the discussion of ^{160}Er.

Table 3: Transitions in ^{160}Er

$\mathbf{E}_\gamma$	$\mathbf{I}_\gamma$ **spin-5 Norm**		$\mathbf{I}_\gamma$ 1^- **Norm**		$\mathbf{E}_i$	$\mathbf{E}_f$
This work	**This work**	**Singh**	**This work**	**Strusny**	**This work**	
125.6	70.5	72.0	8.1	35.0	125.6	0.0
263.8	100.0	100.0	11.3	9.4	389.4	125.6
375.5	28.1	27.0	1.4		764.9	389.4
389.0			0.0	0.7		
463.7	6.3		0.1		1228.6	764.9
520.2			0.1	0.5		
527.1			0.3	0.8	1535.0	1007.6
544.4			0.1		1672.4	1128.0
547.7			0.4	0.6	1535.0	986.9
550.7	7.5		0.1		1315.6	764.9
597.3	3.2	2.9	1.7	1.7	986.7	389.4
618.0			1.6	1.6	1007.3	389.4
636.4			0.0	0.8		
639.8			1.0	1.6	1493.8	854.3
664.8			0.6	0.8	1651.7	986.9
681.2			0.4	0.7	1535.0	854.3
694.0			0.4			

Continued on next page

Table 3 – continued from previous page

E_γ	I_γ spin-5 Norm		I_γ 1^- Norm		E_i	E_f
This work	This work	Singh	This work	Strusny	This work	
728.5			13.4	12.8	854.3	125.6
733.4	15.4		0.2		1498.3	764.9
738.6	7.1	12.0	1.9		1128.0	389.4
752.9			0.5		1645.1	892.2
766.7			2.8	2.9	892.2	125.6
797.6			1.7	2.7	1651.6	854.3
810.2	5.5		0.1		1575.1	764.9
818.3			0.3		1672.4	854.3
839.4	5.0	3.8	0.3		1229.5	389.4
854.2			8.9	8.1	854.3	0.0
861.3	18.8	12.0	7.0	7.0	986.9	125.6
882.1	5.1	2.5	2.8	2.2	1007.6	125.6
926.7	13.0	6.7	0.7		1316.1	389.4
985.3			1.3	0.9	1375.1	389.4
990.4	4.7				1755.3	764.9
999.4			0.9	0.7	1388.8	389.4
1002.7			0.4		1128.0	125.6
1008.0		2.3	4.0	2.5	1008.0	0.0
1082.9	10.1				1847.8	764.9
1104.0	12.5	5.3	0.6	0.6	1229.5	125.6
1114.9	10.9	5.0	0.5		1504.3	389.4
1130.7	4.7				1895.6	764.9
1140.6	6.3					
1152.6			1.2	1.1		

Continued on next page

Table 3 – continued from previous page

E_γ	I_γ spin-5 Norm		I_γ 1^- Norm		E_i	E_f
This work	This work	Singh	This work	Strusny	This work	
1186.4	12.0	4.2	0.7		1575.8	389.4
1249.6	19.6	6.5	2.1	2.8	1375.0	125.6
1264.4			0.8	1.3	1388.8	125.6
1269.7			2.8	3.0	1393.3	125.6

4.3.1 Conversion electron spectroscopy of $^{160}_{68}$Er from the decay of $^{160}_{69}$Tm

With a few exceptions (^{98}Mo etc), the first excited state of an even-even nucleus is a 2^+ state, with an E2 transition to the 0^+ ground state. Conversion electron spectroscopy provides multipolarity information for nuclear transitions. An example of the use of conversion electron spectroscopy to obtain multipolarity information for an E2 transition is illustrated using the 126 keV transition in the ground-state band of ^{160}Er. The conversion electron peaks shown in Figure 23 are in coincidence with the 264 keV γ ray.

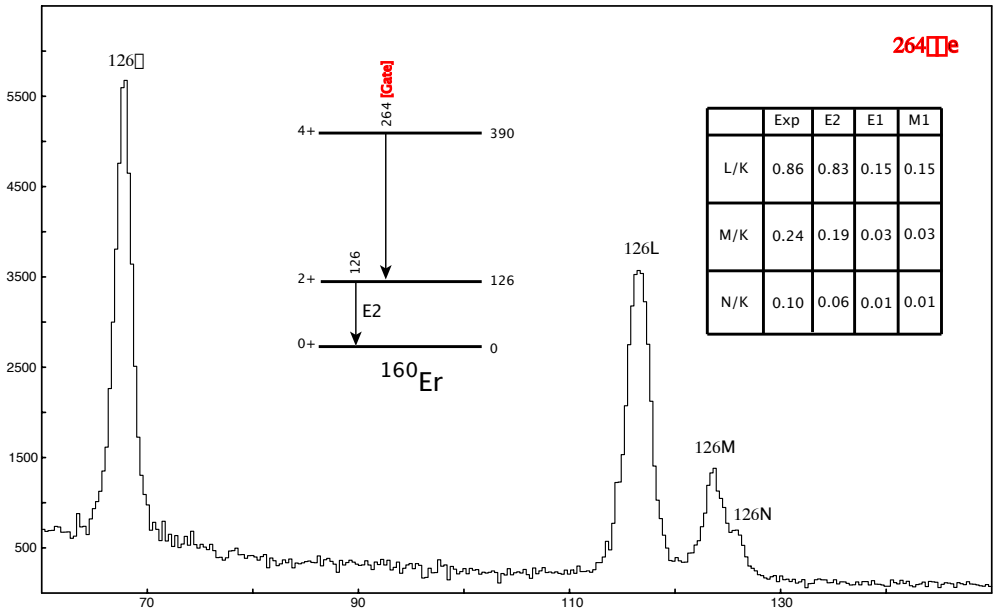

Figure 23: Coincidence gate on the 264 keV γ-ray displaying the conversion electrons observed in the PACES detector array.

Figure 23 displays four conversion electron peaks associated with the 126 keV transition. The K,L,M, and N electron peaks of the 126 keV transition are all distinct and the background is flat, allowing Gaussian fits to be made for these peaks. The areas of these peaks are used to obtain multipolarity information for the transition.

The table embedded in Figure 23 shows relative intensities of the 126K,L,M,N lines obtained from experimental peak areas. Next to the experimental ratios are the theoretical predictions for E2, M1, and E1 transitions. The theoretical predictions are from BRICC [2]. The table shows agreement between the experimental ratios and the E2 theoretical calculations. This method of deducing multipolarity information is used to make spin and parity choices for excited states in the present study.

4.4 Spectroscopy of $^{160}_{69}Tm$ from the decay of $^{160}_{70}Yb$

The production of ^{160}Yb by spallation leads to the β-decaying ground state, $T_{1/2} = 4.8$ min, $J^{\pi} = 0^{+}$. Figure 14 displays the previously established decay scheme. The nucleus $^{160}_{69}\mathrm{Tm}_{91}$ has many low-energy levels because it has an unpaired neutron and an unpaired proton. The spin and parity of these states are determined by these unpaired nucleons. The present study observes many of these levels, through the many γ rays in association with the decay of ^{160}Yb to ^{160}Tm.

Figure 24 displays a log-scale plot of part of the γ-ray spectrum, paired with the corresponding part of the conversion electron spectrum.

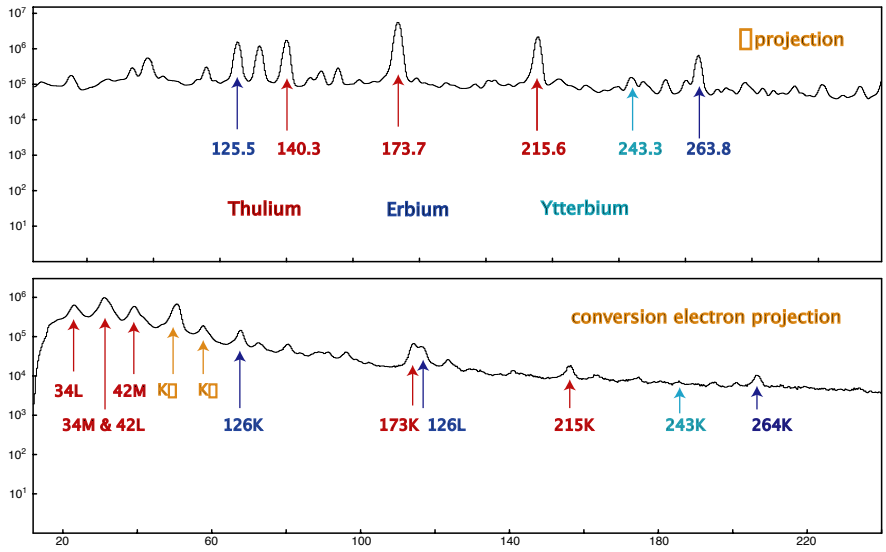

Figure 24: Log-log plot of the γ-ray projection matched with the conversion electron spectrum.

Transitions in the decay of ^{160}Yb to ^{160}Tm are highlighted in red in Figure 24. When comparing the two projections, the number of low-energy conversion electrons in the decay of ^{160}Yb to ^{160}Tm stands out. Transitions belonging to the decay of the other $N = 90$ nuclei are highlighted. Transitions from the decay of ^{160}Yb to ^{160}Tm dominate the spectrum.

A new first-excited state at 34 keV in ^{160}Tm is found in this study, using coincidence information obtained from these low-energy conversion electrons. The associated 34 keV γ ray was observed by Schilling et al. [6], and was placed in coincidence with the 140 keV γ ray, above a level at 140 keV as shown in Figure 14. With the low-energy conversion electron coincidence spectra collected in this study, we can place the 34 keV γ ray below the 140 keV transition in the level scheme, making the 34 keV level the first excited state in ^{160}Tm. Figure 25 shows coincidence spectra supporting this 34 keV level, using a combination of γ-ray and conversion-electron spectroscopy.

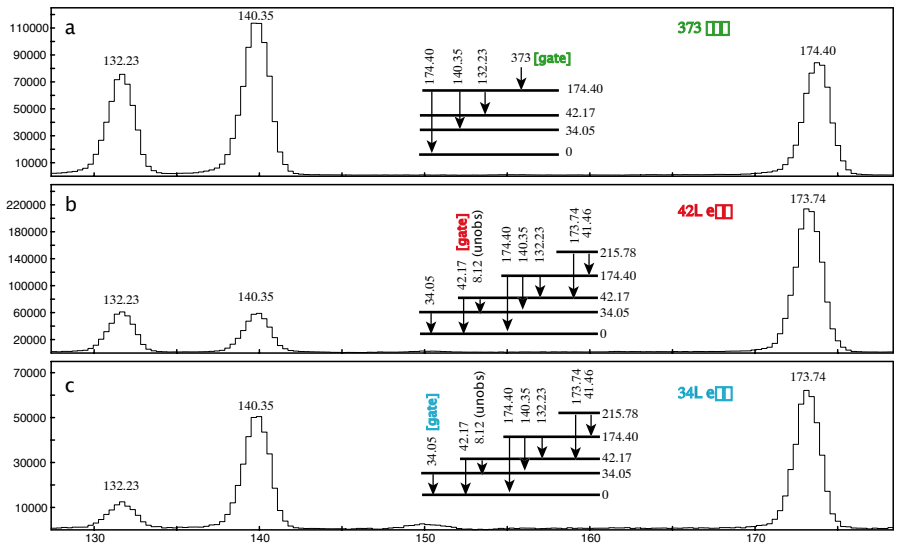

Figure 25: A three-fold γ-ray and conversion-electron coincidence set aimed at elucidating the low-energy level scheme in ^{160}Tm.

Figure 25a displays a coincidence gate on the 373 keV γ ray feeding the level at 174 keV. The 132, 140, and 174 keV γ rays are all very intense in this coincidence gate. Figure 25b displays a coincidence gate on the L-shell electron peak from the 42 keV transition. Figure 25c displays a coincidence gate on the 34 keV L peak. Both of the conversion electron coincidence spectra display the 173 keV γ ray. The 173 and 174 keV transitions would be seen added together, but for the isolation of each through coincidence spectroscopy. This illustrates the sub-keV resolution in the present study, pulling apart the 173.7 keV γ ray from the 174.4 keV γ ray.

Figure 25 suggests a new ordering for the 140 and 34 keV pair of γ rays. The 34 keV γ-ray transition is now placed as de-exciting the 34 keV level to the ground state. This is motivated by the strength of the 173 keV γ ray seen in Figure 25c. Placing the 140 keV γ ray from the level at 174 keV to the level at 34 keV fits more consistently with the

coincidence gates shown.

The 173 keV γ ray is seen in the 34 keV coincidence gate, even though it feeds the level at 42 keV. This is because an unobserved 8 keV transition must exist between the 42 keV level and the 34 keV level. Neither of the detector systems used in this study have detection sensitivity down to 8 keV. The existence of this transition is deduced from the relative strengths of the 132 keV and 173 keV peaks in Figures 25b,c. The ratio of these strong γ rays allows confidence that the 8 keV transition connects the 42 keV level to the 34 keV level.

Preliminary spin and parity information can be established for the energy levels shown in Figure 25 using conversion electron spectroscopy for γ transitions feeding these levels. Figure 26 displays coincidence gates on the 140 and 132 keV transitions, which are directly above the 34 and 42 keV levels, respectively, from the level at 174 keV. These coincidence gates allow preliminary identification of the spin and parity of the levels at 34 and 42 keV.

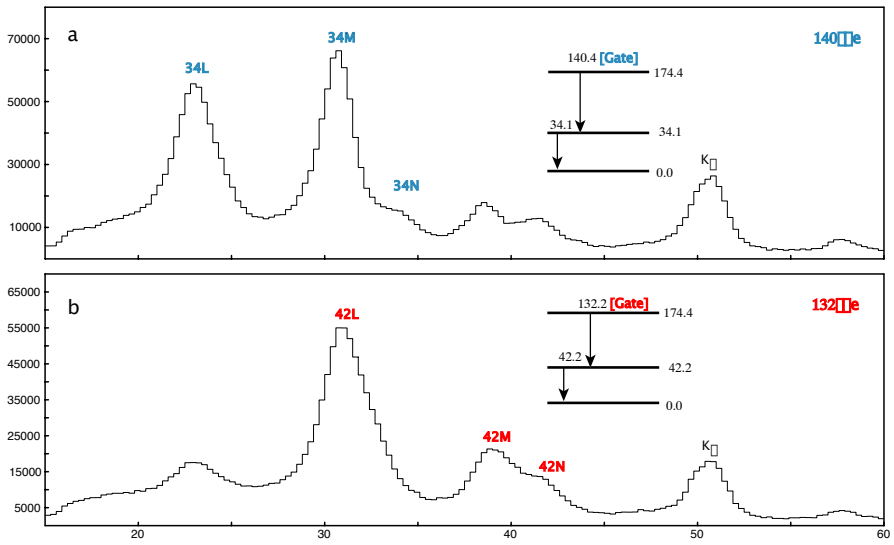

Figure 26: Coincidence gates displaying conversions electrons for the first two excited states in ^{160}Tm, aimed at clarifying spin and parity assignments for the 34 and 42 keV levels.

The 42 keV level is assigned a spin and parity of 2^- by Schilling et al. [6]. The 34 M peak seen in Figure 26a is stronger in comparison to the 34 L peak, than the 42 M peak in Figure 26b is to the 42L peak. This will lead to a difference in the ratio of the area of the L and M peaks, for these two levels. The spin and parity of the level at 34 keV, is deduced from the ratio of the 34M to 34L peak area. The area ratio between the M and L peak for the 34 keV transition is 1.2, which compared with theoretical calculations gives no clear indication of a multipolarity assignment. Making spin and parity assignments to a new level is an iterative process. Partial information is gained from one set of coincidence gates, then we return to assigning this 34 keV level a spin and parity once other coincidence gates have been analyzed. This step by step process will use different γ rays feeding the 34 keV level, and by comparing their M peak to L peak ratio, additional information can assist in reaching a conclusion. The area ratio between the M and L peaks for the 42 keV

transition is 0.15 which, compared with theoretical calculations, indicates an E1 transition. This leads to an assignment of 2^- for the 42 keV state, consistent with assignment of this level from the work of Schilling et al. [6].

The ground state of ^{160}Tm has spin and parity 1^- [1]. This, along with the many low-lying 1^+ energy levels (directly fed in the allowed β decay of the 0^+ground state of ^{160}Yb), produces an abundance of electric dipole (E1) transitions, as outlined by Schilling et al. [6].

Now coincidence gating from above on the 373 keV transition feeding the level at 174 keV, isolates the γ rays below the 174 keV level. The 8π system can detect the 174, 140, and 132 keV γ rays, while the conversion electrons from the 34 and 42 keV transitions are only seen by the PACES array.

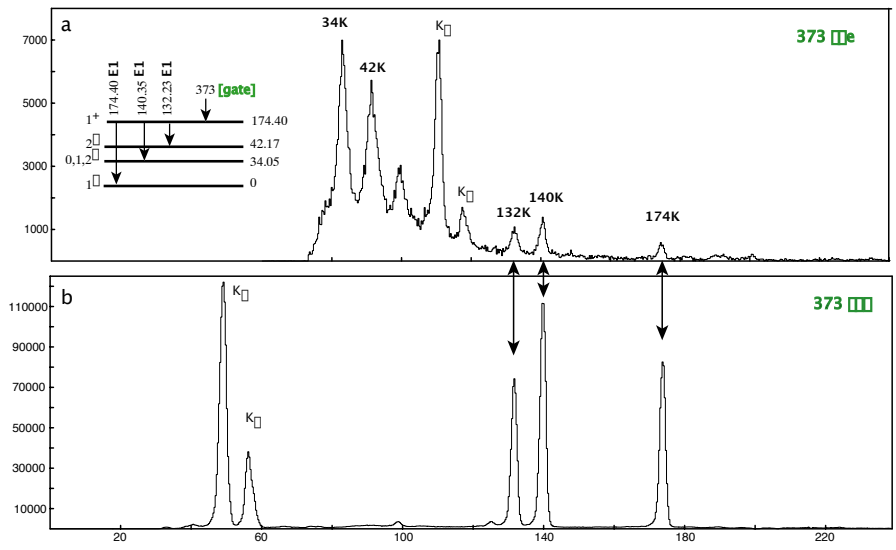

Figure 27: Coincidence gate on the 373 keV γ ray, matched with a conversion electron gate on the 373 keV γ ray, illustrating the 132, 140, and 174 keV transitions.

Figure 27a shows the conversion electron peaks in coincidence with the 373 keV transition, shifted by the K-shell binding energy of 59.6 keV so that the peaks line up with the γ ray peaks below them in Figure 25b. The first few states are summarized in the inset level diagram, indicating spin and parity information for the levels involved from the work of Schilling et al. [6]. The appearance of clear K-shell peaks for the 132, 140, and 174 keV γ rays, with no substantial L-shell peak, is consistent with the ratio in area between these two peaks for an E1 transition. The 132, 140 and 174 keV transition were assigned as E1 transitions by Schilling et al. [6].

A change in level structure from the previous work is motivated by the feeding of the 215 keV level. To see γ rays feeding the level at 215 keV, we will first use a coincidence gate from below.

Schilling et al. [6] have many different γ rays feeding the 215 keV level, as outlined in Figure 14. A coincidence gate on the 215 keV γ ray is shown in Figure 28.

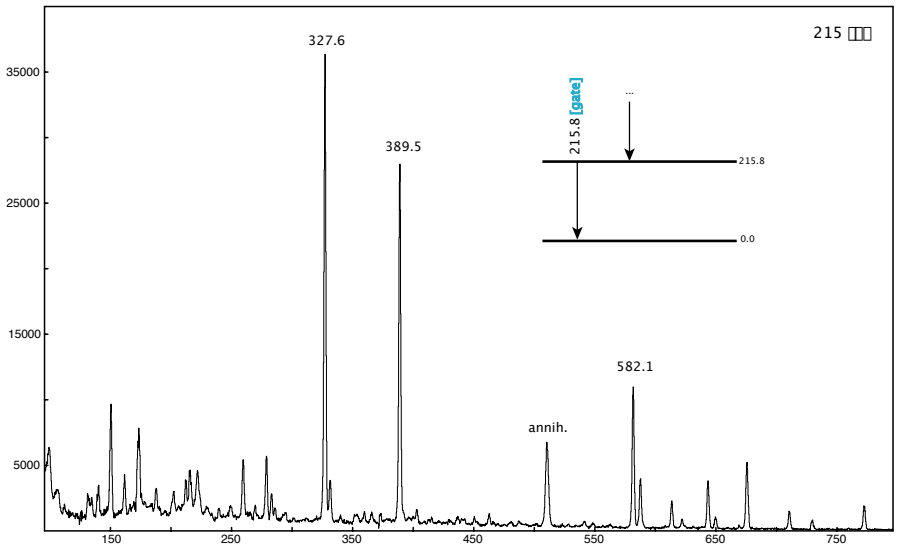

Figure 28: Coincidence with the 215 keV transition in ^{160}Tm, displaying feeding of the 215 keV level.

The strength of the 327 and 389 keV peaks in the 215 keV coincidence gate places these two transitions as directly feeding into the 215 keV level. The coincidence gates for each γ ray individually however, reveals a more complicated feeding.

Figure 29a,b displays coincidence gates for the 327 and 389 keV γ rays respectively.

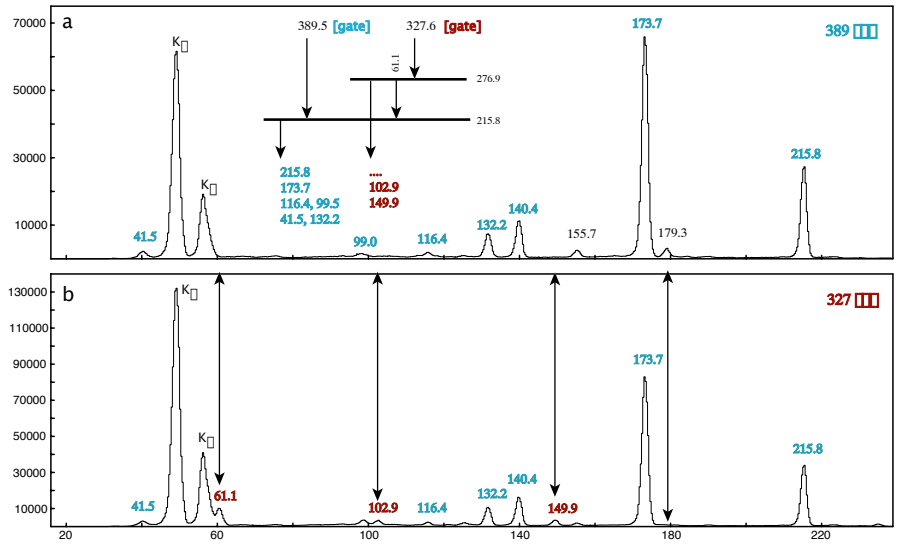

Figure 29: Coincidence gate on the 389 keV γ ray matched with a gate on the 327 keV γ ray

Figure 29 identifies the 61 keV transition in coincidence with 327 keV transition. The 61 keV transition was placed by Schilling et al. [6] out of a level at 605 keV. The coincidence information shown here supports a placement of this 61 keV transition directly into the 215 keV level. Outlined by the diagram inset in Figure 29a, the placement of the 327 keV transition is not directly into the 215 keV level but into the newly established level at 276 keV. With the 61 keV transition into the 215 keV level, Figure 29b then isolates the 103 keV and 149 keV transitions out of the 276 keV level.

The existence of a new energy level in ^{160}Tm at 276 keV, motivated by the new placement of the 61 keV γ ray, affects the placement of several γ rays in the ^{160}Tm decay scheme. Information about additional transitions into the level at 276 keV is presented in Figure 30 through a coincidence gate on the 61 keV γ ray.

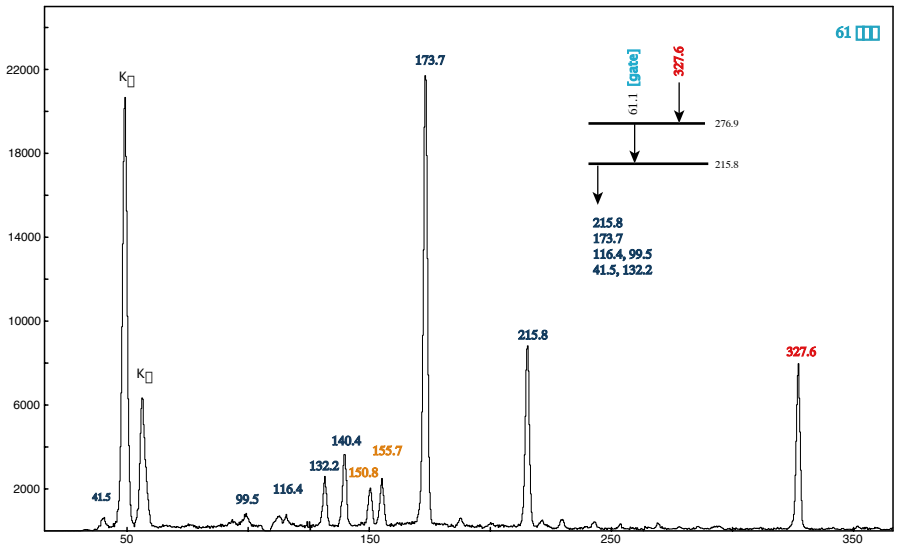

Figure 30: Coincidence gate on the 61 keV γ ray feeding the level at 215 keV

Figure 30 uses colors to identify the known transitions below the 215 keV level, in order to isolate new transitions into the level at 276 keV. This coincidence information prompts a new placement of the 327, 582, and 588 keV γ rays in the decay of ^{160}Yb to ^{160}Tm. The 150 and 155 keV γ rays were identified as in coincidence with a 62 keV transition from higher in the decay scheme. A running gate is used again to assign particular γ rays in coincidence with either the 61 or 62 keV transition, respectively.

Figure 31 summarizes the changes in the level diagram of ^{160}Tm resulting from the present study, viz: the re-ordering of the 34 keV and 140 keV γ-ray pair, and the movement of the 327, 582, and 588 keV γ rays as feeding the new level at 276 keV.

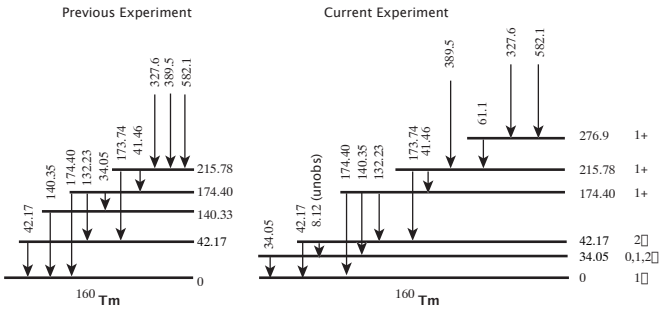

Figure 31: Low-energy level scheme for ^{160}Tm, highlighting changes resulting from the present study.

The new levels at 34 and 276 keV are given preliminary spin and parity assignments, based on multipolarity information. Table 4 shows a comparison between the present study and the work of Schilling et al. [6], listing the energies and intensities of γ rays assigned to the ^{160}Yb to ^{160}Tm β decay.

Table 4: Transitions in Tm

$\mathbf{E}_\gamma$		$\mathbf{I}_\gamma$		**Levels**	
Present study	**Schilling**	**Present study**	**Schilling**	E_i	E_f
34.2	34.2	4.4	3.1	34.1	0.0
41.5	41.5	1.1	0.4	215.8	174.4
42.0	42.0	10.8	7.3	42.2	0.0
59.8		1.3		215.8	155.8
62.1	62.1	2.0	0.5	276.8	215.8
75.4		0.9		174.4	99.4
94.3	94.3	0.7	0.9	268.2	174.4
98.2	98.2	2.6	2.8		
99.5	99.5	2.0	2.1	99.4	0.0
103.2		0.1		276.8	174.4
116.4	116.4	1.9	2.0	215.8	99.4
132.2	132.2	12.3	14.0	174.4	42.2
140.4	140.4	19.2	22.2	174.4	34.4
155.8	155.8	1.8	1.7	155.8	0.0
169.7		0.1		268.2	99.4
173.7	173.7	100.0	100.0	215.8	42.2
174.4	174.4	14.5	13.2	174.4	0.0
178.8		0.1		276.8	99.4
215.8	215.8	43.4	48.0	215.8	0.0
225.8		0.2		494.5	268.2
270.3		0.1		547.4	276.8
278.7	278.0	0.8		494.5	215.8
279.5		0.7	1.0	547.7	268.2
312.2		1.0		859.3	547.4

Continued on next page

Table 4 – continued from previous page

E_γ		I_γ		Levels	
Present study	**Schilling**	**Present study**	**Schilling**	E_i	E_f
318.1		0.4		865.2	547.4
320.0	320.0	3.2	3.4	494.5	174.4
327.6	327.6	6.0	5.6	605.4	276.8
331.8		0.5		547.4	215.8
354.6	354.6		1.1		
356.9	356.9		0.7		
365.0		0.3		859.3	494.5
366.1	366.2	0.9	1.1	634.5	268.2
371.0	373.0	0.1		865.2	494.5
373.0	386.3	10.1	10.0	547.4	174.4
386.3			3.0		
389.5	389.5	6.5	5.2	605.4	215.8
395.2	395.2	0.9	1.6	494.5	99.4
397.0		0.8		891.6	494.5
398.2		0.8		945.8	547.4
429.0	429.0		1.2		
441.2		0.8		987.2	547.4
447.9		0.1		547.4	99.4
451.1		0.6		945.8	494.5
462.3		0.2		677.5	215.8
465.2	465.2		1.4		
490.1		0.1		1037.7	547.4
543.2		0.2		1037.7	494.5
563.1	563.1		1.8		

Continued on next page

Table 4 – continued from previous page

E_γ		I_γ		Levels	
Present study	**Schilling**	**Present study**	**Schilling**	E_i	E_f
578.9		0.1		677.5	99.4
582.1	582.1	4.4	3.0	859.3	276.8
588.7	588.7	1.6	1.5	865.2	276.8
613.9		0.9		891.6	276.8
622.1		0.1		891.6	268.2
643.8		1.6		859.3	215.8
650.0		0.4		865.2	215.8
675.9		2.1		891.6	215.8
685.2		0.3		859.3	174.4
691.3		0.3		865.2	174.4
710.9		0.8		987.2	276.8
729.7		0.4		945.8	215.8
760.3		0.1		859.3	99.4
772.9		1.9		945.8	174.4
772.8		1.1		987.2	215.8
814.5		0.2		987.2	174.4
821.9		0.4		1037.7	215.8

4.5 Changes to level schemes of ^{160}Tm

The decay of ^{160}Yb to ^{160}Tm observed in this study is very complex. The elucidation of this decay involved coincidence gates on hundreds of individual γ-ray transitions. Table 4 displays the observed transitions reported by the present study, detailed with coincidence intensity information normalized to reference intensities [1]. A normalization was required for each coincidence gate because absolute intensity information was unavailable, therefore only coincidence intensities are reported. For each decay a single reference [1] was used, this allows the production of intensity information for most γ-ray transitions observed.

The most significant changes to the level scheme of ^{160}Tm are outlined with displayed figures in the previous section. The elucidation of the finer details of this decay are summarized starting with the removal of previously reported levels.

The level at 140.33 keV reported with a tentative $0^+, 1^+, 2^+$ spin and parity assignment is removed by the present study. This level was reported as fed by a 34 keV transition from the 174 keV level and drained by a 140 keV transition to the ground state. As Figure 25 displayed this study motivated a new ordering for these 2 transitions, ultimately removing the reported level at 140 keV.

The level at 543.36 keV reported with no spin and parity information is also removed by the present study. This level was drained by the 327 keV transition to the 215 keV level. Figure 29 displayed the difference between the 389 keV transition (confirmed as directly feeding the level at 215 keV) and the 327 keV transition. These differences in coincidence between two transitions reported as feeding the same level motivated a change in the location of the 327 keV transition, and removal of the reported level at 543 keV.

4.5.1 Excited states in ^{160}Tm

This study corroborates 8 of the 10 reported excited states in ^{160}Tm at 42, 99, 174, 215, 494, 547, 605 and 797 keV. In addition to observing these reported excited states, this study adds many new levels (shown in Figure 34) with tentative spin and parity assignments based on transition multipolarity information.

Figure 25 displayed the spectra demonstrating the existence of the excited state at 34 keV. This first excited state is fed primarily by the 140 keV transition from the 174 keV level, and drained by the 34 keV transition to the ground state.

Figure 26 displays conversion-electron spectroscopy information for both the 34 and 42 keV levels. These two low energy levels exhibit a marked difference in spin and parity. The 42 keV level was reported as a 2^- state, and the multipolarity information about the 132 keV transition feeding the level at 42 keV corroborates this spin and parity for the 42 keV level. The multipolarity information about the 34 keV transition draining the new level at 34 keV, suggests this transition is M1 to the ground state.

The 99 keV level previously reported is corroborated by the present study. It is mainly fed by the 116 keV transition from the level at 215 keV and drained by the 99 keV transition to the ground state. This level has additional feeding from the 75, 395, new 578, new 760 and new 766 keV transitions from the 174, 494, new 677, new 859 and new 865 keV levels, respectively. Coincidence intensities are reported for these transitions using the previous 116 keV intensity as a normalization.

The 155 keV level is newly reported by the present study. A 155 keV transition was reported by the previous work with no position in the decay scheme. The level at 155 keV is primarily fed by a 59 keV transition from the level at 215 keV, and drained by the 155 keV transition to the ground state.

The present work observed the reported transitions out of the 174 keV level as depicted in Figure 25 (notably the 116, 132, 140 and 174 keV transitions). This work reports the addition of several new transitions feeding this level. The 41 keV transition from the 215 keV level is difficult to observe free of intensity contributions from the 42 keV transition. Coincidence intensity information about this transition is reported after removal of the percentage from transitions close in energy. The 103 keV transition, first observed by this work, is established from the new level at 276 keV (introduced with Figure 26) feeding the level at 174 keV. The present study observed additional feeding of the 320, 373, 429, new 623, new 685, new 691, new 772, new 814 and new 979 keV transitions from the 494, 547, 605, 797, new 859, new 865, new 945, new 987 and new 1154 keV levels, respectively.

The present work observed the reported transitions below the 215 keV level as depicted in Figure 30 (notably the 116, 132, 140, 173 and 215 keV transitions. The level is fed by the 61, 279, new 332, 389, 462, new 644, new 650, new 676, new 730 and new 822 keV transitions from the 277, 494, 547, 605, 677, 859, 865, new 891, 945 and new 1037 keV levels, respectively.

The level at 277 keV established by the present study is fed by the new 217, new 270, 327, 582, 588, new 614 and new 710 keV transitions from the 494, 547, 605, 859, 865, 891 and 987 keV levels, respectively. This summarizes the movement of a number of previously reported γ rays in this decay scheme.

The level at 494 keV is fed by several higher energy γ rays including the 365, new 371, new 397, new 451, new 543 and new 660 keV transitions from the 859, 865, 891, 945, 1037 and 1154 keV levels respectively.

The previously reported level at 547 keV is observed in the present study to be additionally fed by the new 312, new 318, new 344, new 398, new 441, new 490 and new 607 keV transitions from the the 859, 865, 891, 945, 987, 1037 and 1154 keV levels respectively.

The depth of investigation in this study was curtailed at the level of .1 units of intensity. This designation of a strongest unplaced γ ray creates a lower limit to the intensities that are discussed herein.

CHAPTER V

DISCUSSION

5.1 Discussion of ^{160}Yb

The nucleus $^{160}_{90}$Yb displays characteristics of a transitional region between vibrational and rotational nuclei. The $N = 90$ nuclei lie on the edge of two well-defined regions of structural characteristics. Figure 32 displays the chart of the nuclides with the identification of regions of nuclear collective structure.

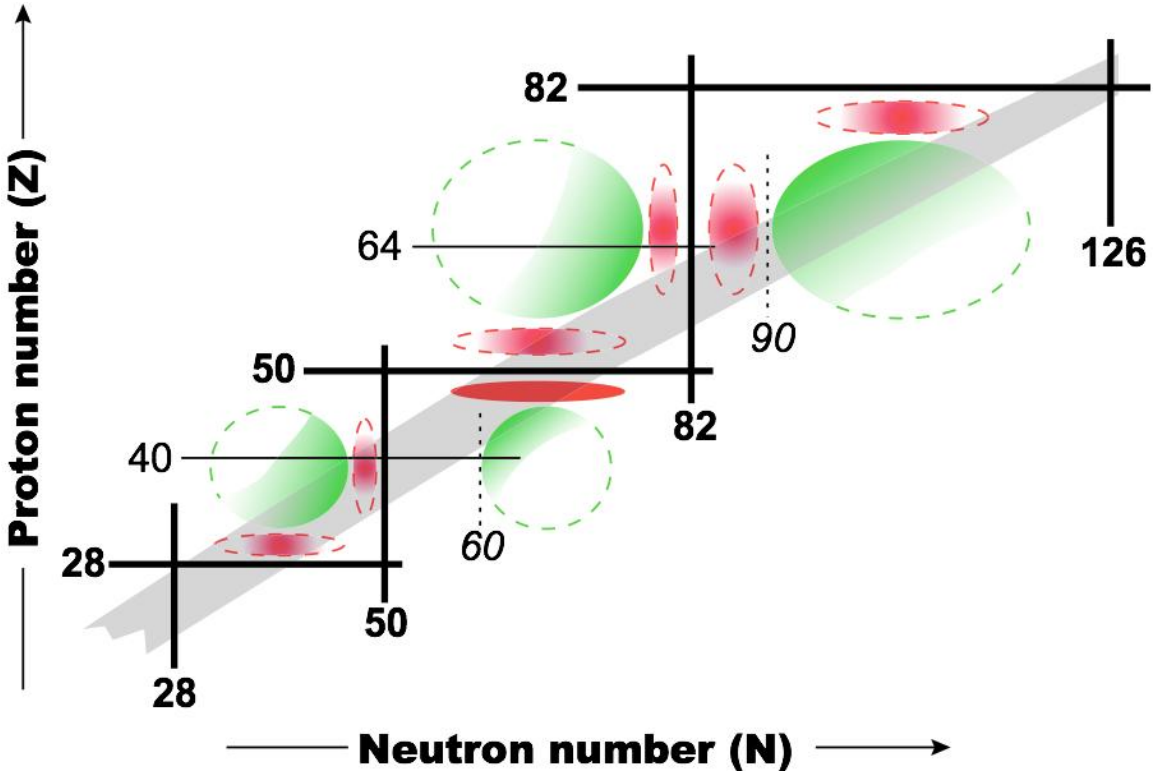

Figure 32: A display showing regions of collective nuclear structure.

The extended gray area in the background of Figure 32 represents the β stable nuclei. The thick lines in Figure 32 are the magic numbers for neutrons and protons. The colored shaded areas represent regions where detailed structural information is known. The transitional $N = 90$ nuclei lie between areas of nuclei whose ground states are classified as either

rotational or vibrational. At $N = 90$ the bands of different deformation are close enough in energy for some states to mix strongly. This causes a repulsion between certain states in these bands. The energy separation of the more deformed band expands while the the spacing of the less deformed bands compresses. The energy bands are then seen with nearly the same energy spacing.

The present study observed the decay of ^{160}Lu to ^{160}Yb using the 8π spectrometer and the PACES array to make a detailed γ-ray spectroscopic analysis. Table 2 provides coincidence intensity information for the known transitions in this decay with appropriate normalization and error bars.

The ground band of ^{160}Yb has a $\frac{E(4^+)}{E(2^+)}$ ratio of 2.6. This ratio is midway between the vibrational limit of 2.0 and the rotational limit of 3.3. The ground band is not populated above the 4^+ state at 638 keV. The 243 keV $2^+_g \rightarrow 0^+_g$ and 395 keV $4^+_g \rightarrow 2^+_g$ transitions are the only in-band γ rays observed.

The level at 820 keV is the 2^+ state in the γ band. This bandhead location is lower in energy for ^{160}Yb than it is for the $N = 90$ nuclei closer to stability. This band continues with the 3^+_γ level at 1112 keV and the possible 4^+_γ level at 1529 keV, with an observed intra-band transition, the 292 keV $3^+_\gamma \rightarrow 2^+_\gamma$ γ ray. Inter-band transitions are observed from these states to the ground band, including the 577 keV $2^+_\gamma \rightarrow 2^+_g$ transition, the 869 keV $3^+_\gamma \rightarrow 2^+_g$ transition, the 1283 keV $4^+_\gamma \rightarrow 2^+_g$ transition, the 474 keV $3^+_\gamma \rightarrow 4^+_g$ transition and the 890 keV $4^+_\gamma \rightarrow 4^+_g$ transition. The 188 keV $2^+_\gamma \rightarrow 4^+_g$ transition is observed, but is very weak due to the branching ratio of the 820 keV state. The present study introduces intensities deduced for these transitions in Table 2.

The level at 1086 keV is the 0^+ state in the β band. This bandhead location is higher in energy for ^{160}Yb than it is for the $N = 90$ nuclei closer to stability. This band continues with the 2^+_β level at 1292 keV. Inter-band transitions are observed from these states to the ground band, including the 843 keV $0^+_\beta \rightarrow 2^+_g$ transition, the 1086 keV $0^+_\beta \rightarrow 0^+_g$ transition,

the 653 keV $2^+_\beta \rightarrow 4^+_g$ transition and the 1049 keV $2^+_\gamma \rightarrow 2^+_g$ transition.

These trends in bandhead location for the $N = 90$ isotones are shown in Figure 4. The nucleus ^{160}Yb lies far from stability in the $N = 90$ nuclides. The present study was directed at observing the excited bands in ^{160}Yb in order to further study the onset of deformation, observed in $N = 90$ nuclei closer to stability. The present study represents the first look at $N = 90$ nuclei far from stability with an array of HPGe detectors, however with the experimental challenges outlined in the production and collection of ^{160}Lu for its decay to ^{160}Yb, little new information is observed. This study corroborates previously reported levels and provides coincidence intensity information normalized to the reported intensity of specific transitions. A normalization is used in order to compare intensities of γ rays for all observed transitions for each decay.

The present study adds one excited state to ^{160}Yb at 1676 keV along with 2 new γ-ray transitions in the decay from ^{160}Lu. With an actinide target, the production of ^{160}Lu would increase and this study could detail this decay in more depth. The intensities for the transitions observed in this decay are listed in Table 2.

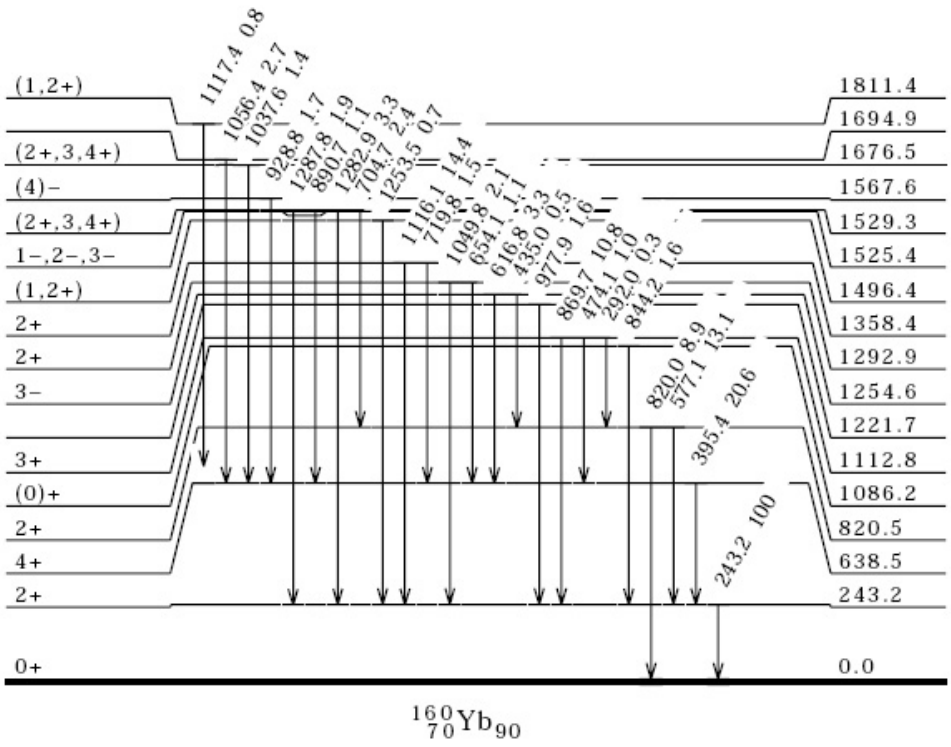

Figure 33: ENSDF style level scheme for ^{160}Yb

Figure 33 summarizes the information the present study adds to the knowledge of the decay of ^{160}Lu to ^{160}Yb.

5.2 Discussion of ^{160}Tm.

The β decay of ^{160}Yb had a very high activity in this study. This allowed for the collection of a large amount of coincidence data that details specific transition information about this decay. Over 50 γ rays are assigned to this decay, with placement of these γ rays in the decay scheme of the daughter nucleus, ^{160}Tm. Energy level rearrangements were made to match observed coincidence information, as well as addition of new transitions between existing levels.

The decay of ^{160}Yb to ^{160}Tm is an example of β decay into an odd-odd nucleus. The depth of investigation in the present work was limited to major changes, because exhaustive detail (at present) offers no new physics.

This work established a level at 34 keV, the new first excited state in ^{160}Tm. Preliminary spin and parity assignments for this level are given in Table 4. Five new levels and 36 new γ rays have been added to the decay of ^{160}Yb to ^{160}Tm.

The new level established at 277 keV, illustrates the elucidation of a complex decay scheme using coincidence information. The 61 keV γ ray was observed by Schilling et al. [6] and placed from the 605 keV level to the level at 544 keV. With the coincidence information in this study we demonstrated that the proper placement of the 61 keV γ ray in the decay scheme is out of the level at 277 keV to the level at 215 keV. The new placement of the 61 keV γ ray moves several other transitions. The 582 and 588 keV γ rays both feed the level at 277 keV. The 859 keV level already existed in the work by Schilling et al. [6], we now match this existing level with the 582 keV γ ray transition into the 277 keV level. The level at 865 keV is reported by the present study, with the 588 keV γ ray being placed into the 277 keV level, these matches strengthen the case for these rearrangements.

The accuracy of the coincidence information from this study is presented using a running gate to pull apart closely-spaced transitions. The 61 keV peak in the projection spectrum is unresolved from the weaker 59 keV transition located lower in the spectrum (the 215→155

keV transition). A number of the transitions observed in this decay required contributions from other transitions removed for an accurate intensity determination to be made. This resulted in a detailed analysis of each coincidence gate used for the intensity calculation. Contributions were found from transitions often times from the decay of neighboring isobar nuclei. The intensities shown in Table 4 have been normalized to reported intensities in order to compare between coincidence gates.

The advances in equipment over recent years to incorporate large scale detector arrays has allowed this study to make many detailed coincidence measurements in this decay. The detector arrays used in the present study provide spectra with a low enough background to distinguish very weak transitions in support of the addition and removal of excited states in ^{160}Tm. This study was able to perform a detailed analysis on the decay of ^{160}Yb to ^{160}Tm correcting and extending the previously reported information.

Conversion electron spectroscopy was able to support the multipolarity assignment of γ-ray transitions in ^{160}Tm. The low-energy nature of many of the excited states and γ-ray transitions makes the detection of conversion electrons by the Si detectors below 50 keV very important. The resolution of low-energy transitions and the ability to make coincidence measurements on higher energy γ-rays using low-energy conversion electrons, made available information for the new level ordering seen in low-energy transitions in ^{160}Tm.

Investigation of the feeding of the levels at 34 and 42 keV in ^{160}Tm is made possible by looking at conversion-electron gated γ-ray spectra. Initially the density of transitions in this decay made elucidation of the level scheme information difficult. The ability to combine sets of coincidence information together allowed questionable assignments based on one type of coincidence spectra to be checked and justified with coincidence information from the second system. The spin and parity of the two levels 34 and 42 keV are different. The present study presents preliminary spin and parity assignments for the rearranged level scheme. Using the electron peak areas, and theoretical comparisons, basic multipolarity information is obtained.

A summary of the new information obtained for the decay of ^{160}Yb to ^{160}Tm is pertinent here. Figure 34 is an ENSDF style rendition of the decay scheme with the removals and additions supported by the present study. The intensity information displayed was calculated on a per coincidence gate basis and normalized to reported intensities in the previous work.

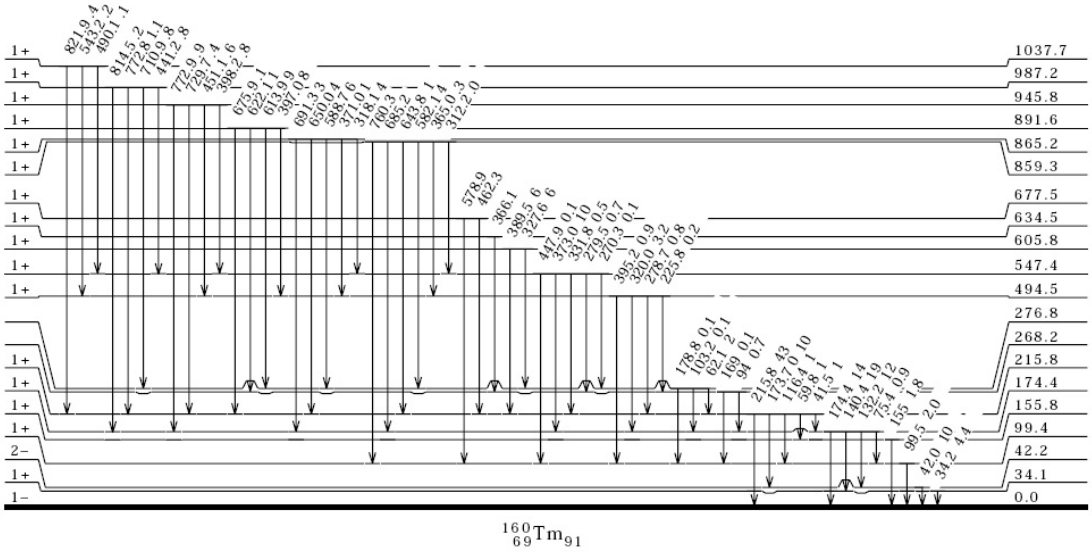

Figure 34: ENSDF style level scheme for ^{160}Tm

The elucidation of the decay into an odd-odd daughter nuclei is a tedious and complicated process. Corroboration of information is necessary when so many coincidence gates involving transitions in this decay include γ rays in coincidence with transitions of similar energy. The γ-rays seen in coincidence spectra can be recognized first and foremost by the energy of coincident x rays. This is helpful in this study because coincident peaks are often confusing and unexpected if the transition of similar energy belongs to the decay of a different nucleus.

Figure 35 displays how transitions can be identified by their x-ray coincidences. All the γ-ray transitions of a particular isobaric decay will show in a coincidence gate centered on the K_α x-ray energy of that decay.

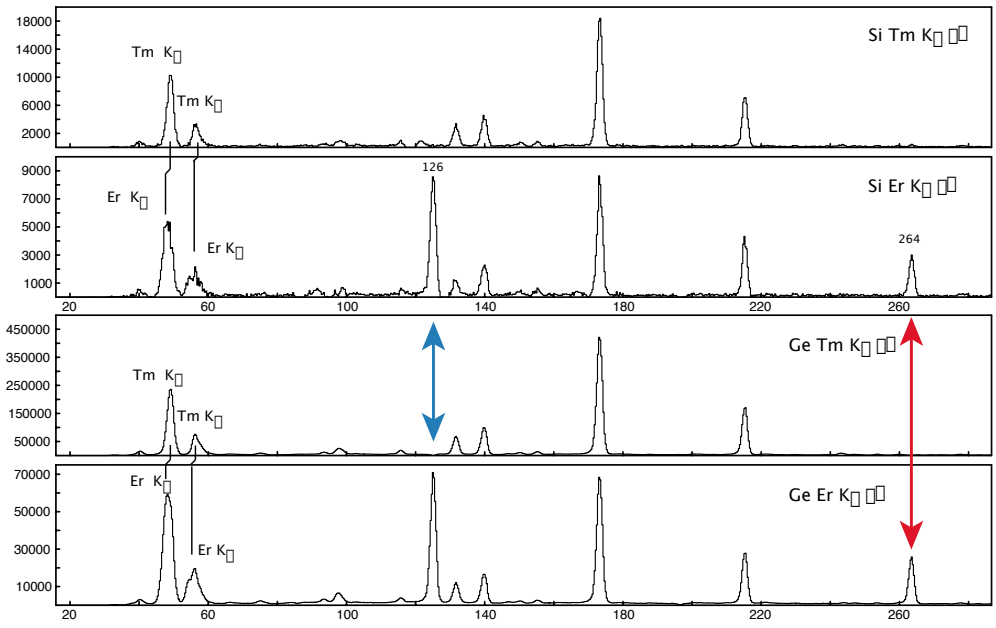

Figure 35: A pair of spectra from each detector system displaying γ rays in coincidence with K_α x-rays from the decay of ^{160}Yb to ^{160}Tm and ^{160}Tm to ^{160}Er, respectively.

This demonstrates a simple method to identify the decaying isobar to which a particular observed transition belongs. This is important for properly placing transitions and excited states seen in coincidence with weak transitions so that a misidentification of coincidences isn't made. The transitions in the decay of ^{160}Tm to ^{160}Er often required removal of intensity contributions from the many transitions in the decay of ^{160}Yb to ^{160}Tm.

5.3 Discussion of ^{160}Er.

Figure 15 and Figure 16 display the decays of ^{160}Tm to ^{160}Er. The two β decaying isomers involved and the subsequent γ-ray decays of the daughter nucleus are shown. The first excited 2^+ state in ^{160}Er is at 126 keV, which indicates that it is a strongly deformed nucleus. The structural interest in ^{160}Er is its behavior as a standard rotor. This study presents a comparison of the rotational characteristics of ^{160}Er with neighboring Erbium isotopes. The investigation of ^{166}Er has been previously carried out to make a precision test of the rotational model [18]. A correlation between ^{160}Er and ^{166}Er, a well described rotor, allows conclusions to be made regarding the rotational structure of ^{160}Er.

This study corroborates 12 of the 16 excited states in ^{160}Er at 125, 389, 854, 893, 987, 1007, 1374, 1389, 1395, 1494, 1535 and 1652 keV as reported by Strusny et al. [7] and Bykov et al. [8]. The spin-5 decay observed in the present study populated additional levels at 765, 1128, 1230, 1316, 1505 and 1576 keV. The spectra shown in the ^{160}Er results section demonstrate the population of these excited states in ^{160}Er.

In ^{160}Er one notices that, besides a low-lying $K = 2$ band with a bandhead at 854 keV (very similar to the above mentioned ^{166}Er which has a $K = 2$ band at 786 keV), there is a low-lying excited $K = 0$ band at 894 keV. The ground, β and γ bands are observed to be populated to at least $J = 6$ in this study. This allows a careful analysis to be done on the cascade of many transitions in the decay of ^{160}Tm to ^{160}Er.

The 125 keV 2_g^+ state previously reported[1] is observed by the present study, fed by many transitions and drained by the 125 keV transition to the ground state. The feeding mainly includes the 264 keV transition from the level at 389 keV. Additional feeding is observed from the 728, 767, 861, 882, 1003, 1103, 1249, 1264 and 1269 keV transitions from the 854, 893, 987, 1007, 1128, 1229, 1374, 1389 and 1395 keV levels, respectively. Table 3 displays coincidence intensities calculated for these transitions using a normalization intensity from the previous work on the spin-1 and spin-5 decay for comparison.

The 389 keV 4_g^+ state previously reported[1] is observed by the present study, fed by transitions from level populated by both the spin-1 and spin-5 decay. The spin-5 decay transitions include the 375, 597, 738, 840, 926, 1115 and 1186 keV transitions from the 765, 987, 1128, 1230, 1316, 1505 and 1576 keV levels, respectively. The spin-1 decay transitions additionally include the 617, 985 and 999 keV transitions from the 1007, 1374 and 1389 keV levels, respectively. This coincidence gate also uses both calculated normalizations for comparison with feeding from both the spin-1 and spin-5 decays. Transitions first observed in this work feeding this level include the 1247 keV transition from a state at 1637 keV with a tentative 4^- spin and parity and the 1153 keV transition from a level at 1542 keV.

The 765 keV 6_g^+ state is only fed by the spin-5 decay. The present study observed the 464, 551, 734, 739, 810, 975, 990, 1083 and 1131 keV transitions feeding this level from the 4_β^+ 1229, 5_γ^+ 1317, spin-5 1500, spin-5 1506, spin-6 1577, 7_γ^+ 1742, spin-6 1757, spin-6 1850 and 4^+ 1897 keV levels, respectively.

The 854 keV 2_γ^+ state is fed by both the spin-1 and spin-5 decays. The present study observes the 275, 617, 640, 681, 731, 797, 818 and 843 keV transitions feeding this level from the 4_γ^+ 1128, spin 2 1472, spin 2 1496, 2^+ 1535, spin 3 1586, spin 2 1653, $3_{\beta\gamma}^+$ 1674, spin 3 1698 and 4^+ 1897 keV levels, respectively.

The 893 keV 0_β^+ state is fed by the spin-1 decay. The present study observes the 641 and 753 keV transitions feeding this level from the 2^+ 1535 and 2^+ 1648 keV levels, respectively.

The 987 keV 3_γ^+ state is fed by both the spin-1 and spin-5 decays. The present study observes the 328, 402, 507, 548, 597, 664, 709 and 908 keV transitions feeding this level from the 5_γ^+ 1317, spin 2 1390, spin 2 1496, 2^+ 1535, spin 3 1586, spin 2 1653, spin 3 1698, and 4^+ 1897 keV levels, respectively.

The 1007 keV 2_β^+ state is fed by both the spin-1 and spin-5 decays. The present study observes the 527 and 665 keV transitions feeding this level from the 2^+ 1535 and $3_{\beta\gamma}^+$ 1674 keV levels, respectively.

The 1128 keV 4^+_γ state is fed primarily by the spin-5 decay. The present study observes the 371, 376, 407, 457, 544, 568 and 767 keV transitions feeding this level from the spin 5 1500, spin 5 1506, 2^+ 1535, spin 3 1586, $3^+_{\beta\gamma}$ 1674, spin 3 1698 and 4^+ 1897 keV levels, respectively.

The 1230 keV 4^+_β state is fed primarily by the spin-5 decay. The present study observes the 312, 417 and 444 keV transitions feeding this level from the 6^+_β 1542, spin 2 1648 and $3^+_{\beta\gamma}$ 1674 keV levels, respectively.

The 1317 keV 5^+_γ state is fed by the spin-5 decay. The present study observes the 579 and 587 keV transitions feeding this level from the 4^+ 1897 and 6^- 1907 keV levels, respectively.

The present study adds 8 levels and 13 γ-rays to the decay of ^{160}Tm to ^{160}Er. The level scheme developed for this study combines the levels and transitions from both the spin-5 and spin-1 decays. The coincidence intensity is reported and specific normalization is applied where feeding can be isolated to either decay.

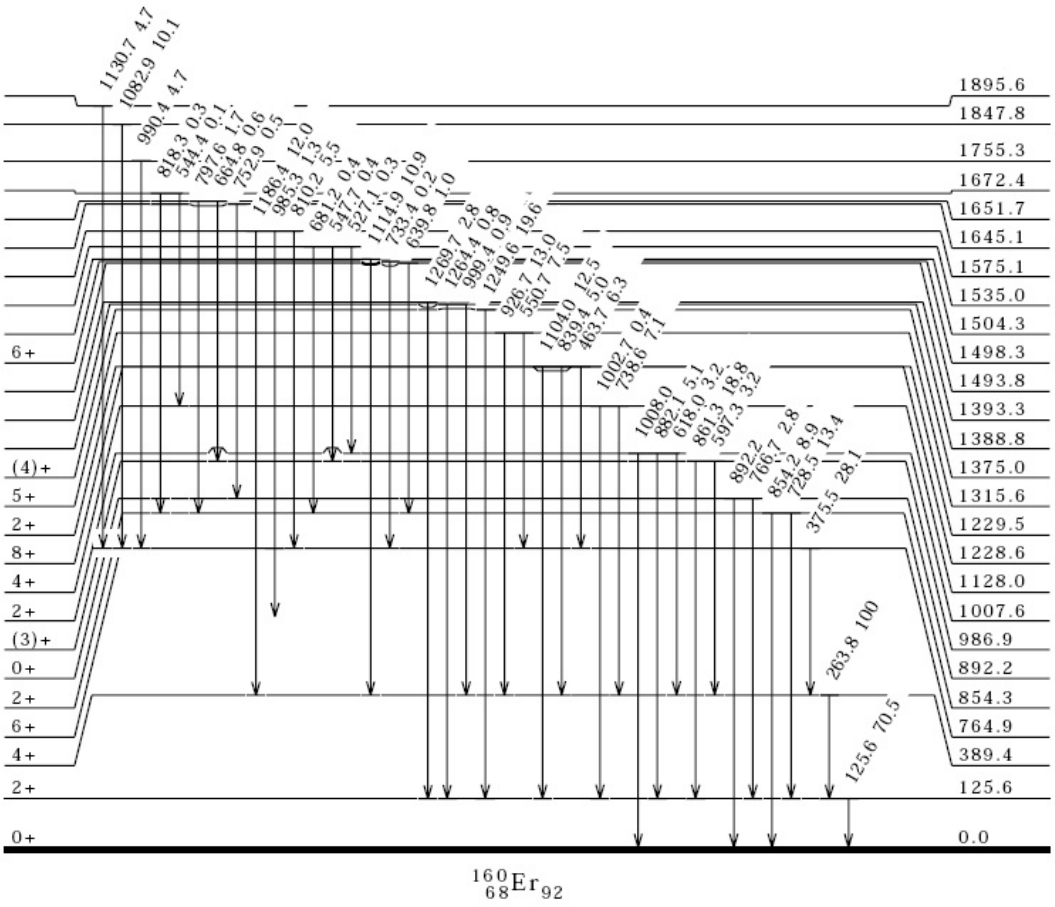

Figure 36: ENSDF style level scheme for ^{160}Er

5.3.1 Mikhailov plot generation for ^{160}Er

The comparison of the rotational characteristics of ^{160}Er is done using a Mikhailov plot [18]. These plots measure the transition probability vs. magnitude of spin change to classify rotational properties of interband transitions in nuclei. The $Z = 68$ isotopes higher than $N = 90$ are closer to stability and have conclusive deformed structural aspects that we can use for comparison with the present work. Table 3 outlines the γ-ray transitions reported by the present study and these intensities are used in the calculation of the transition probabilities. The reduced transition probability is given by

$$P(I_i K_i \rightarrow I_f K_f) = \frac{\sqrt{\frac{I_\gamma}{(E_\gamma)^5}}}{\langle I_i K_i 2\mu | I_f K_f \rangle} \tag{35}$$

where $\mu = K_f - K_i$ and the denominator is a Clebsch-Gordan coefficient. The magnitude of spin change delta $\Delta = J_f(J_f + 1) - J_i(J_i = 1)$, is calculated for the various inter-band transitions observed in this decay.

Figure 37 shows the Mikhailov plot generated for ^{160}Er using data from the present study. The γ-ray transitions used to make this plot include the $4_\gamma \rightarrow 4_g$ 740 keV transition, the $4_\gamma \rightarrow 2_g$ 1003 keV transition, the $5_\gamma \rightarrow 6_g$ 551 keV transition, the $5_\gamma \rightarrow 4_g$ 927 keV transition, the $6_\gamma \rightarrow 6_g$ 734 keV transition, the $2_\gamma \rightarrow 2_g$ 728 keV transition and the $2_\gamma \rightarrow 0_g$ 854 keV transition. Table 3 lists the energies and intensities of these inter-band transitions along with the rest of the γ rays assigned to the decay of ^{160}Tm to ^{160}Er.

To make a precision test of the rotational characteristics of ^{160}Er, we can compare the Mikhailov plot generated by the present study to the well-described rotor ^{166}Er. The Mikhailov plot shown in Figure 38 was obtained from the study of Kulp et al. [18]. The nucleus ^{166}Er is well described as having a strongly-deformed nuclear shape.

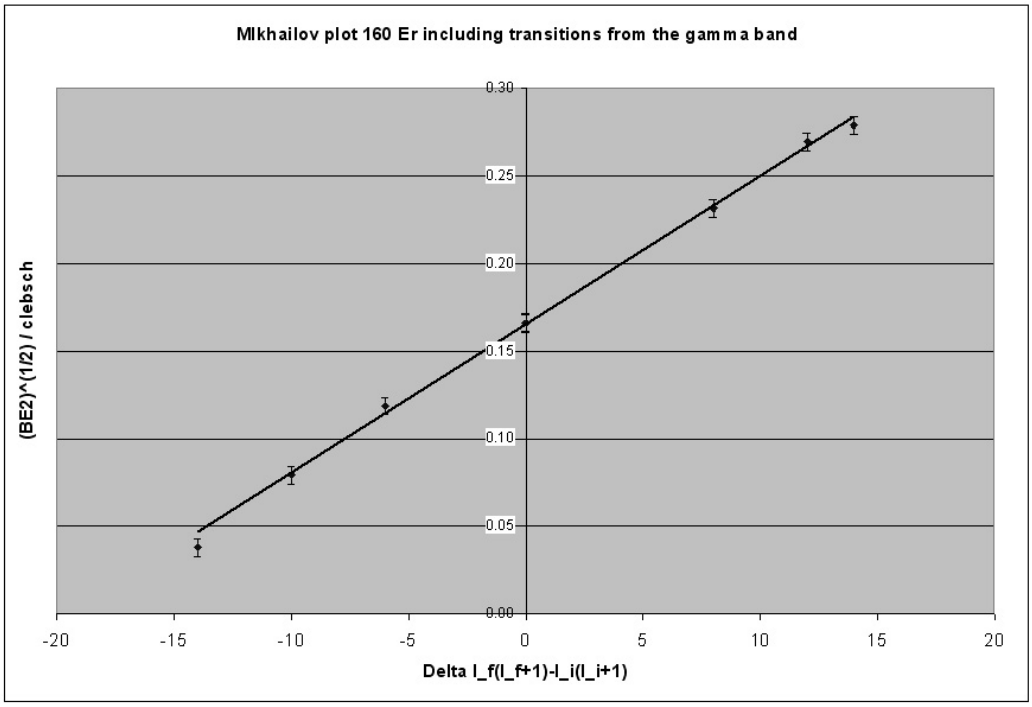

Figure 37: Mikhailov plot for ^{160}Er

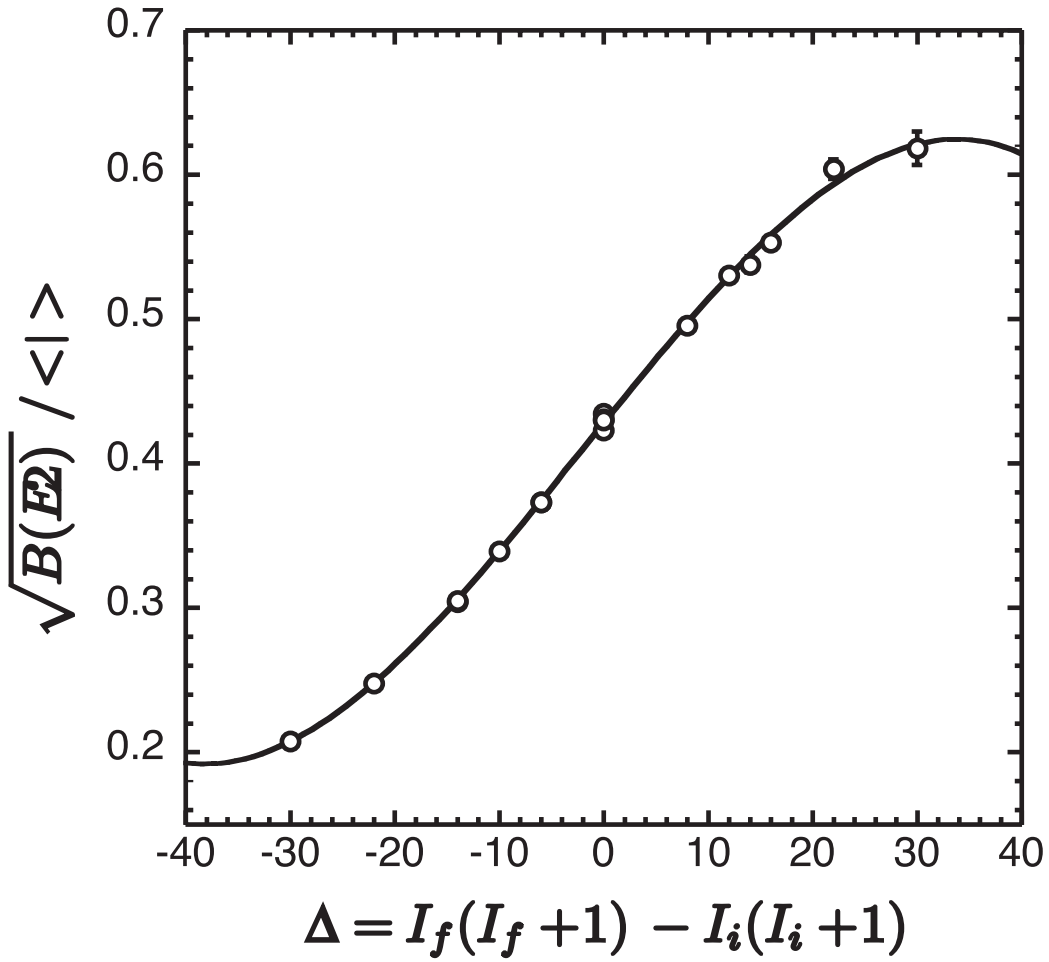

Figure 38: Mikhailov plot for ^{166}Er

The differences between Figure 37 and Figure 38 arise from the difference in the $K = 0$ bands of these nuclei. The nucleus ^{160}Er has a level scheme influenced by mixing in the $2_\beta - 2_\gamma$, $4_\beta - 4_\gamma$, and $6_\beta - 6_\gamma$ states.

CHAPTER VI

CONCLUSIONS

6.1 Implication of results

New states have been added to the level structure of ^{160}Tm and tentative levels which were previously reported [1] are critically reviewed. This study reports intensities for several $A = 160$ nuclei through β decay of mass-separated sources. The present study demonstrates that a very complex decay scheme can be elucidated using γ-ray and conversion-electron spectroscopy.

Conversion-electron coincidence gating enables very low-energy level structure to be observed. A new first excited state was found at 34 keV in ^{160}Tm and several other reported transitions (327,582 and 588) were moved when a 61 keV transition was re-assigned to feed the 215 keV level from a new level at 277 keV. Conversion-electron - γ-ray coincidence have been used only very rarely in far from stability studies.

Coincidence measurements obtained from multiple detector systems enabled multipolarity assignments to transitions and detailed levels with spin and parity selections. The configuration of the 8π-PACES spectrometers which included the five Si conversion-electron detectors, allowed γ-e^- coincidences to assist in the placement of transitions. In addition multipolarity information about transitions observed in this study were supported with conversion electron coincidences intensities. The combination of these systems introduced information about many previously reported states with the addition of spin and parity assignments. Coincidence measurements of conversion electrons have not been previously reported in the $A = 160$ region far from stability.

Several levels were added and removed from the decay of ^{160}Yb to ^{160}Tm. These additions were corroborated with multipolarity information from the coincidence of conversion electrons with γ rays. The theoretical subshell ratios for specific types of transitions (E1,E2,M1) were used in comparison to the experimentally observed subshell ratios to determine spin and parity information for energy levels and multipolarity assignment for transitions.

The present study also demonstrates that even closer to stability, i.e., ^{160}Tm $\rightarrow$ ^{160}Er, new information can be obtained. The γ-ray branches between the γ band and the ground band are examined with high-statistics data. The Mikhailov plot generated for ^{160}Er consolidates the known information. The tentative spin assignments for higher-energy levels are reviewed using the intensity of interband transitions in comparison to the Clebsch-Gordan coefficient to deduce proper band placement. The $K = 0$ β-band levels are recognized from the $K = 2$ γ-band levels by the difference in strength feeding the ground band. The $K = 0$ levels have strong feeding to higher spin states in the ground band because of the Clebsch-Gordan coefficient differences. Interband transitions from the $K = 2$ band have almost no feeding to higher spin states in the ground band. The knowledge of the excited band structure in ^{160}Er was extended by the present work.

6.2 Future Experiments

The $N = 90$ region of nuclei continue to be a challenge to model theoretically. The sensitivity of current detector arrays offer ranges of additional information about the decay of nuclei far from stability. The current study represents the caliber of data that is obtained when a large array of detectors is used to collect information about a very complex decay. The 8π represents a significant advance in both efficiency and solid angle coverage over the detector systems utilized in previous studies. The precision of these systems allows careful deduction of the proper placement of transitions and the addition or removal of energy levels for these nuclei.

The present study observed the decay of ^{160}Lu $\rightarrow$ ^{160}Yb with statistics no better than the published work. This type of experiment needs an actinide target to avoid the production problems observed for ^{160}Lu from a ^{181}Ta target.

Many closely-spaced doublets in the decay of ^{160}Yb $\rightarrow$ ^{160}Tm were resolved, and intensity contributions from each were separated. With every transition observed below $\approx$400 keV, contributions from γ-ray transitions of similar energy were present. The present work uses coincidence gating to resolve the transitions of individual nuclei. This enables studies of isobaric chains far from stability. Isobaric decay chains far from stability will have ^{A}Z (even-even) $\rightarrow$ ^{A}Z-1 (odd-odd) daughter nuclei which are extremely complex. The coincidence method utilized in the present study yields intensities of very weak transitions which could not be resolved in singles data.

REFERENCES

[1] Evaluated Nuclear Structure Data File (ENSDF) Database Manager: Jag Tuli, NNDC, Brookhaven National Laboratory, International Network of Nuclear Structure and Decay Data Evaluators ;

[2] BRICC conversion coefficient calculator, T. Kibdi, T.W. Burrows, M.B. Trzhaskovskaya, P.M. Davidson, C.W. Nestor, Jr. 'Evaluation of theoretical conversion coefficients using BrIcc' Nucl. Instr. and Meth. A 589 (2008) ;

[3] H.Auer, J.Fernandez-Niello, H.Puchta, F.Riess Z.Phys. A **318**, 323 (1984).

[4] O.Haxel, J.H.D.Jensen and H.E.Suess Phys. Rev. **75** (1949) 1766.

[5] W.Gelletly, Nucl.Instrum.Methods **211**, 89 (1983).

[6] I. Adam, W. Andrejtscheff, T. M. Muminov, H. U. Siebert, R. R. Usmanov and Yu. V. Yushkevich, K. D. Schilling, Nuclear Physics A. **311**, 1-2 (1978).

[7] H.Strusny, H.Tyrroff, E.Herrmann, G.Beyer, K.Y.Gromov, T.A.Islamov, M.Jachim, H.-U.Siebert, S.A.Usmanova, Czech.J.Phys. **25**B, 626 (1975).

[8] A.A.Bykov, V.D.Vitman, Yu.V.Naumov, S.Yu.Orlov, V.K.Tarasov, Izv.Akad.Nauk SSSR, Ser.Fiz. 46, 2230 (1982); Bull.Acad.Sci.USSR, Phys.Ser. 46, **11**, 166 (1982).

[9] B. Singh Phys. Rev. C **28**, 2118 - 2121 (1983).

[10] K. Dusling and C. Vaman, Phys Rev C **73**, 014317 (2006).

[11] J. Rainwater, Phys. Rev. **79**, 432 (1950);
J. Rainwater, Rev. Mod. Phys. **48**, 385 (1976).

[12] A. Bohr, Kongl. Dan. Vid. Selsk. Mat.-fys. Medd. **26**, no. 14 (1952);
A. Bohr, Rev. Mod. Phys. **48**, 365 (1976).

[13] G. Alaga, K. Alder, A. Bohr, and B.R. Mottelson, Mat. Fys. Medd. Dan. Vid. Selsk. **29**, no. 9 (1955).

[14] V.M. Mikhailov, Izv. Akad. Nauk SSSR, ser. fiz. **28**, 308 (1964) [transl. Bull. Acad. Sci. USSR, phys. ser. **28**, 225]; *ibid.* **30**, 1334 (1966) [transl. **30**, 1392].

[15] A. Bohr and B.R. Mottelson, Nuclear Structure, Vol. 1 and Vol. 2 (W.A. Benjamin, Inc., Reading, Ma, 1975).

[16] A.S. Davydov and G.F. Filippov, Nucl. Phys. **8**, 237 (1958).

[17] A.S. Davydov, At. Energy Rev. **6**, 3 (1968).

[18] W.D. Kulp, Ph.D. dissertation, Georgia Institute of Technology, (2001).

[19] J.L. Wood, A.M. Oros-Peusquens, R. Zaballa, J.M. Allmond, and W.D. Kulp, Phys. Rev. C **70**, 024308 (2004).

VITA

Nathaniel Joseph Brown was born in Saranac Lake, New York to parents Richard R. Brown Jr. and Mary Patricia Brown. He was raised in rural Cooperstown, New York (along with older brother Jeremiah, and younger sister Elizabeth) in the heart of upstate New York.